Review Article

Improving the understanding and performance of clinical MRI using tissue property filters and the central contrast theorem, MASDIR pulse sequences and synergistic contrast MRI

Ya-Jun Ma[1], Dina Moazamian[1], Daniel M. Cornfeld[2,3], Paul Condron[2,3], Samantha J. Holdsworth[2,3], Mark Bydder[1], Jiang Du[1,4,5], Graeme M. Bydder[1,2]

[1]Department of Radiology, University of California San Diego, San Diego, CA, USA; [2]Mātai Medical Research Institute, Tairāwhiti-Gisborne, New Zealand; [3]Department of Anatomy and Medical Imaging and Centre for Brain Research, Faculty of Medical and Health Sciences, University of Auckland, Auckland, New Zealand; [4]Research Service, Veterans Affairs San Diego Healthcare System, San Diego, CA, USA; [5]Department of Bioengineering, University of California San Diego, San Diego, CA, USA

Contributions: (I) Conception and design: All authors; (II) Administrative support: YJ Ma, SJ Holdsworth, J Du; (III) Provision of study materials or patients: YJ Ma, D Moazamian, DM Cornfeld, P Condron, SJ Holdsworth; (IV) Collection and assembly of data: YJ Ma, D Moazamian, DM Cornfeld, P Condron; (V) Data analysis and interpretation: YJ Ma, D Moazamian, DM Cornfeld, P Condron, M Bydder; (VI) Manuscript writing: All authors; (VII) Final approval of manuscript: All authors.

Correspondence to: Graeme M. Bydder. Department of Radiology, University of California San Diego, 9452 Medical Center Drive, San Diego, CA 92037, USA. Email: gbydder@health.ucsd.edu.

Abstract: This paper updates and extends three previous papers on tissue property filters (TP-filters), Multiplied, Added, Divided and/or Subtracted Inversion Recovery (MASTIR) pulse sequences and synergistic contrast MRI (scMRI). It does this by firstly adding the central contrast theorem (CCT) to TP-filters, secondly including division with MASTIR sequences to make them Multiplied, Added, Subtracted and/or Divided IR (MASDIR) sequences, and thirdly incorporating division into the image processing needed for scMR to increase synergistic T_1 contrast. These updated concepts are then used to explain and improve contrast at tissue boundaries, as well as to develop imaging regimes to detect and monitor small changes to the brain over time and quantify T_1. The CCT is in two parts: the first part states that contrast produced by each TP is the product of the change in TP multiplied by the TP sequence weighting which is the first partial derivative of the TP-filter. The second part states that the overall fractional contrast is the algebraic sum of the fractional contrasts produced by each of the TPs. Subtraction of two IR sequences alone about doubles contrast relative to a conventional single IR sequence. Division of this subtraction can amplify contrast 5–15 times compared with conventional IR sequences. Dividing sequences can be problematic in areas where the signal is zero but this is avoided by dividing the difference in signal of two magnitude reconstructed IR sequences by the sum of their signals. The basis for the production of high contrast, high spatial resolution boundaries at white-gray matter junctions, between cerebral cortex and cerebrospinal fluid (CSF) and at other sites with subtracted IR (SIR) and divided subtracted IR (dSIR) sequences is explained and examples are shown. A key concept is the tissue fraction f, which is the proportion of a tissue in a mixture of two tissues within a voxel. Contrast at boundaries is a function of the partial derivative of the TP-filter, the partial derivative of the relevant TP with respect to f, and the partial derivative of f with respect to distance, x. Location of tissue boundaries is important for segmentation and is helpful in determining if inversion times have been chosen correctly. In small change regimes, the high sensitivity to small changes in T_1 provided by dSIR images, together with the high definition boundaries, afford mechanisms for detecting small changes due to contrast agents, disease, perfusion and other causes. 3D isotropic rigid body registration provides a technique for following these changes over time in serial studies. Images showing high lesion contrast, high definition tissue and fluid boundaries, and the detection of small changes are included. T1 maps can be

created by linearly scaling dSIR images.

Keywords: MRI; central contrast theorem; MASDIR pulse sequences; synergistic contrast MRI (scMRI); contrast at tissue boundaries; small change regimes; T_1 quantitation; multiple sclerosis (MS)

Submitted Apr 20, 2022. Accepted for publication May 31, 2022.
doi: 10.21037/qims-22-394
View this article at: https://dx.doi.org/10.21037/qims-22-394

Introduction

This paper follows three previous ones on tissue property filters (TP-filters) (1), MASTIR (Multiplied, Added, Divided and/or Subtracted Inversion Recovery) pulse sequences (2) and synergistic contrast MRI (scMRI) (3). It documents progress in each of these areas, and utilizes concepts common to each of them to describe new approaches to understanding and improving contrast at tissue boundaries as well as the use of imaging regimes to study small changes in the brain and quantify T_1.

The concept of TP-filters has been extended and formalized as the central contrast theorem (CCT) and its corollaries. These are derived from the Bloch, Torrey and Larmor equations. They formalize the contribution to contrast from changes in TPs as well as sequence weighting for individual TPs, and uses the algebraic sum of the fractional contrasts produced by different TPs to determine overall fractional contrast.

The MASTIR sequences have been extended by the inclusion of division to the other three basic operations of arithmetic namely addition, subtraction and multiplication. Fitting of inversion recovery (IR) sequences which was included previously is now treated as a separate, but related category. Division has its own issues when the signal of an IR sequence in the denominator of a signal equation is zero. For the particular case of two subtracted IR (SIR) filters with different TIs this problem can be resolved by using magnitude reconstruction and dividing the difference in signal from the two sequences by the sum of their signals. If the filters have different TIs, their sum is non-zero. Division in this way also provides normalization, and can substantially increase the contrast produced by the two SIR sequences compared with that produced by subtraction alone. To include division, the sequences are described as Multiplied, Added, Subtracted and/or Divided IR (MASDIR).

For scMRI, division has been included since it can substantially increase synergistic T_1 contrast and image processing has been formalized so that synergistic contrast can be achieved for any change in sign (i.e., increase or decrease) in disease of each of the three TPs T_1, T_2 and D*. This can be utilized with specific protocols for the brain, as well as other organs and tissues.

Integration of the concepts of TP-filters, MASDIR sequences and scMRI is used to analyze contrast at boundaries and to generate high contrast between white and gray matter boundaries as well as those between cortical gray matter and cerebrospinal fluid (CSF). This involves sequence weightings as well as two other partial derivatives, namely the change in TP with tissue fraction (f), and the change in f with distance, where f is the fraction of one tissue in a mixture of two tissues within a voxel.

The very high sensitivity of particular MASDIR sequences to small changes in T_1 lends itself to detection of small changes in signal and space in images of the brain, as well as monitoring changes in both signal and space over time in serial MRI studies when isotropic 3D acquisitions are used with rigid body registration.

This paper begins with a consideration of normal TPs, how these change in disease, and the effect of contrast agents on them.

Normal TPs, changes of TPs in disease and the effects of contrast agents

There are twenty or more TPs which affect MR images and a critical part of MRI is relating differences/changes in the TPs in disease to contrast seen on MR images. This is described as the central contrast problem in MRI. It requires a knowledge of pulse sequences and pulse sequence parameters to link differences/changes in TPs to differences/changes in signal i.e., contrast (*Table 1*).

It is useful to display the full extent of the values of TPs encountered in clinical practice along the X axis. Differences or changes in a TP between two tissues can then be represented as horizontal green arrows (*Figure 1*). Subsequent understanding of image signal and contrast then

Table 1 The central contrast problem

$\Delta TP,\ \frac{\Delta TP}{TP}$	Pulse sequences and their pulse sequence parameters	Signal (S), phase (θ)
$\Delta\rho_m,\ \frac{\Delta\rho_m}{\rho_m}$	Spin echo (TR, TE...) IR (TR, TI, TE...) PSGE (TR, TE, b...)	$C_{ab} = \Delta S$ $C_{fr} = \frac{\Delta S}{S}$ $\Delta\theta$ = absolute phase contrast
$\Delta T_1,\ \frac{\Delta T_1}{T_1}$		
$\Delta T_2,\ \frac{\Delta T_2}{T_2}$		
$\Delta D^*,\ \frac{\Delta D^*}{D^*}$		
$\Delta\chi$, susceptibility	SGE (TR, TE, α...)	
$\Delta\delta$, chemical shift		
$\Delta\frac{T_2}{T_1},\ \frac{\Delta\frac{T_2}{T_1}}{\frac{T_2}{T_1}}$	Balanced steady state free precession (TR, TE, α...)	
$\Delta UltrashortT_2,\ \frac{\Delta UltrashortT_2}{T_2}$	UTE (TR, TE, α...)	
Δ Flow, Δv	PSGE (TR, TE, δ, Δ ...)	
Δ GBCA concentration c, Δc	SE, IR, SGE, UTE, etc.	

TPs and their differences/changes (ΔTP, $\frac{\Delta TP}{TP}$); pulse sequences and their pulse sequence parameters; signal (S) and phase (θ), signal contrast (absolute contrast C_{ab} = ΔS, fractional contrast $C_{fr} = \frac{\Delta S}{S}$) and phase contrast ($\Delta\theta$ = absolute phase contrast). The central contrast problem is to relate differences/changes in TPs (left column) to differences/changes in signal or phase or contrast (right column) through knowledge of the pulse sequences and their sequence parameters (central column). Conventionally this is done with the concept of weighting which is qualitative, and designates the single TP thought most responsible for the contrast. Frequently more than one TP is responsible for contrast between the different tissues imaged, and pulse sequences have difference sensitivities to TPs. This complexity leads to inconsistencies when using a single TP and qualitative weighting to interpret MR images. SE, spin echo; TP, tissue property; IR, inversion recovery; PSGE, pulsed gradient spin echo; SGE, spoiled gradient echo; UTE, ultrashort TE.

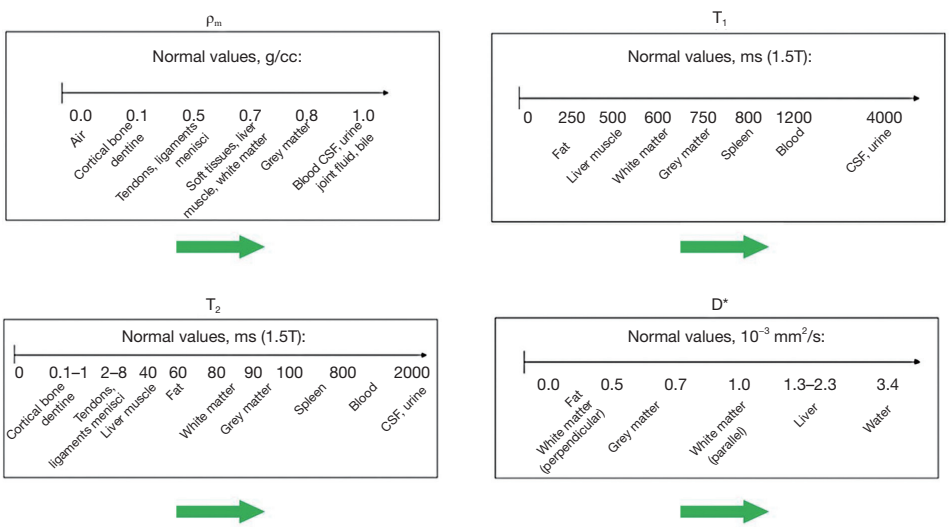

Figure 1 Normal tissue properties ρ_m, T_1 , T_2 and D* ordered from zero to their maximum values along the X axis using a linear X scale. Difference/change in tissue properties are shown as green arrows along the horizontal (X) axis.

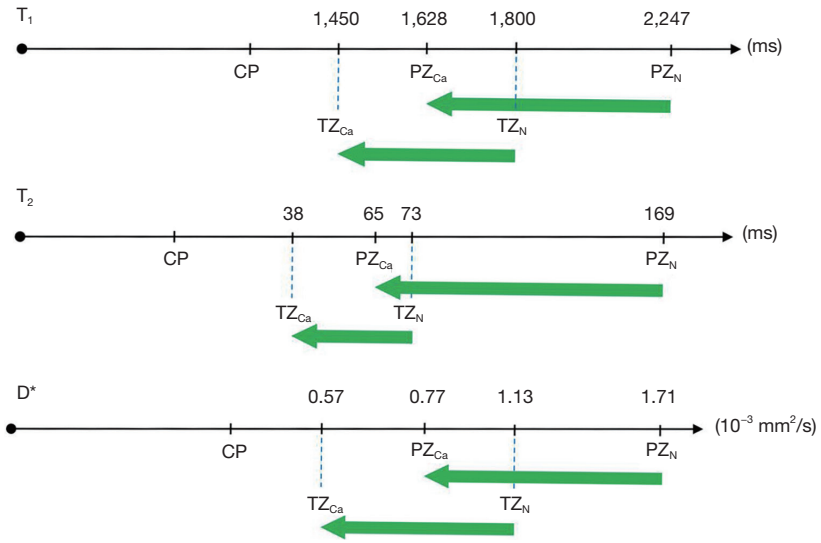

Figure 2 Mean values of T_1 (upper), T_2 (middle) and D* (lower) in normal PZ_N, normal TZ_N and CP (assumed) as well as values of T_1, T_2 and D* in PZ_N and TZ_N in cancer i.e., PZ_{Ca} and TZ_{Ca}. Each of T_1, T_2 and D* is decreased in both the PZ and TZ in changing from normal to cancer (negative horizontal green arrows). The decreases in TPs are substantial, and greater in the PZ than in the TZ. CP, prostate capsule; PZ, peripheral zone; TZ, transition zone.

includes all tissues and fluids visualized on the images. The TP X axis can be either linear or logarithmic. The domain can be chosen to include particular tissues and fluids of clinical interest although for example, with susceptibility, values for metal are far outside those of tissues (In the subsequent text, the term "tissues" is assumed to include fluids unless otherwise stated).

For many diseases (e.g., inflammation, demyelination, tumors, etc.) T_1 and T_2 are increased, but in other conditions, including, for example, hemorrhage and iron deposition, T_1, T_2 and T_2* are often decreased. Diffusion is frequently decreased in acute disease of the brain (infarction, infection) and in many tumors, but increased in other tumors and chronic disease.

For particular applications, it is useful to focus on the relevant tissues and changes in them in disease. *Figure 2* illustrates normal values of T_1, T_2 and D* in the prostate as well as changes in these TPs in tumors. Primary prostate tumors are unusual in that they show a decrease in T_1 and T_2 (as well as the more common decrease in D* in tumors) (4,5). The size of the changes is larger in the PZ than in the TZ and the fractional change is greater for T_2 and D* than it is for T_1.

The signs and magnitudes of the changes in TPs as shown in *Figure 2* are also important for scMRI. If concurrent changes in different TPs are present (which is usually the case), there is an opportunity to use appropriate sequences and image processing to make each of the changes in TP contribute synergistically to the overall contrast of images irrespective of the sign of those changes. The magnitude of the changes in TPs is also important in assessing their relative importance as sources of contrast.

Fluid properties are important in imaging the brain, for example, and often establish the upper or lower points of the image display dynamic range. Partial volume effects between very long T_1 and T_2 CSF and normal tissues may simulate increases in T_1 and T_2 in tissue and thus lesions. For this reason, it is often useful if CSF signals are selectively reduced when heavily T_2-weighted sequences are used. This can be done with techniques such as CSF nulling (T_2-FLAIR sequence) and late echo subtraction (les) (MASDIR sequences). Ideally these techniques should not reduce contrast between the tissues of primary clinical interest.

Pulse sequences as TP-filters and the CCT

The central contrast problem

The central contrast problem in clinical MRI is to relate differences/changes in TPs such as $\Delta\rho_m$, ΔT_1, and ΔT_2 (or

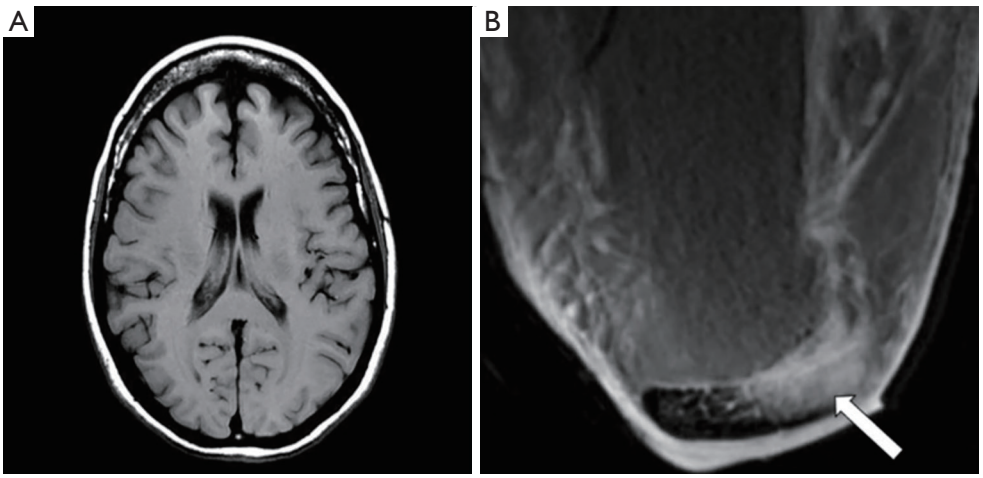

Figure 3 Brain showing normal white matter and gray matter (A), and Achilles tendon showing normal and abnormal (white arrow) areas (B) examined with the same T_1-wSE sequence. The sequence is T_1-weighted for white and gray matter in (A) where the increase in T_1 from white matter (white color) to gray matter (gray color) results in negative contrast. However, the same "T_1-wSE" sequence is T_2-weighted for the Achilles tendon in (B). The increase in T_2 from normal (black, low signal) to abnormal tissue (white, high signal) in the tendon results in high positive contrast (white arrow) (B). If the sequence is regarded as T_1-weighted in the Achilles tendon, the high signal abnormality could be attributed to a decrease in T_1 and therefore be due to hemorrhage, fat and/or GBCA enhancement. In fact, the abnormality is due to an increase in T_2 and is likely to be due to completely different pathology e.g., degeneration, trauma and/or edema. GBCA, gadolinium-based contrast agent.

fractional changes in these TPs $\frac{\Delta\rho_m}{\rho_m}$, $\frac{\Delta T_1}{T_1}$ and $\frac{\Delta T_2}{T_2}$) (*Table 1*, left column) to differences/changes in signal S i.e., contrast Cab = ΔS (or fractional contrast Cfr = $\frac{\Delta S}{S}$) as well as phase θ and differences in phase ($\Delta\theta$) (*Table 1*, right column). This is done via knowledge of the relevant pulse sequences and pulse sequence parameters (*Table 1*, central column). Although the Bloch equations describing MRI relate S to TPs, the primary interest in clinical practice is in relating differences/changes in S (i.e., contrast) to differences/changes in TPs.

The conventional way of doing this is to use qualitative weighting. This designates a single TP as the one thought to be most responsible for the contrast of interest, and describes sequences and images accordingly as, for example, "T_1-weighted", "T_2-weighted" and "diffusion-weighted". However, contrast is often dependent on differences/changes in more than one of the ten TPs shown in *Table 1*. In addition, there are also at least six classes of pulse sequences and these display varying sensitivities to differences/changes in TPs. There are also differences within pulse sequence classes which depend on sequence parameters. This complexity leads to inconsistencies with qualitative weighting when only a single TP is used to describe the relationship between differences/changes in several TPs and the contrast they produce.

Problems with qualitative weighting

Examples of the problems encountered with the use of qualitative weighting include:

(i) A sequence which is T_1-weighted in one application, for example showing contrast between white and gray matter in the brain, can be T_2-weighted in other applications (such as showing contrast between normal and diseased tissue in the Achilles tendon) even though the sequence is still usually described as a T_1-weighted image in this particular application (*Figure 3*).

(ii) T_2-FLAIR sequences are highly T_2-weighted for the brain but are simultaneously highly T_1-weighted for CSF.

(iii) "Diffusion weighted" sequences may be more T_2-weighted than diffusion weighted.

(iv) Although reducing TE is said to reduce T_2-weighting,

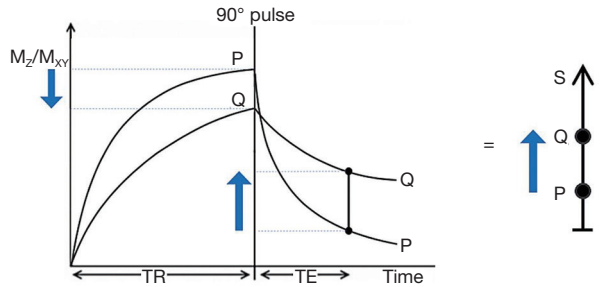

Figure 4 Plot of M_Z/M_{XY} *vs.* time for the SE sequence for two tissues P (with a shorter T_1 and T_2) and Q (with a longer T_1 and T_2). T_1-dependent contrast (first negative blue arrow on left), and overall T_1 and T_2 contrast (second = third positive blue arrows in center and on right) are shown.

subtracted ultrashort TE (UTE) sequences with UTEs (i.e., 8 ms) can be highly T_2-weighted.

(v) "Fluid sensitive" sequences used in the musculoskeletal system are insensitive to fluids such as pore water and matrix bound water in cortical bone. On the other hand, UTE subtraction sequences that are sensitive to pore and matrix bound water are insensitive to joint and bursal fluid.

These and other inconsistencies complicate the use of qualitative weighting for image interpretation in clinical practice, and limit its usefulness for understanding more complex sequences as well as developing new applications of sequences for clinical MRI.

In order to resolve these problems, it is necessary to recognize the fact that several different TPs usually determine contrast with most pulse sequences, and provide specific relationships between difference/changes in TPs and difference/changes in signal (i.e., contrast) with these sequences. This is outlined in the next sections.

The spin echo (SE) sequence

The usual explanation of image signal and contrast with the SE sequence utilizes the Bloch equations. Firstly, it follows longitudinal magnetization (M_Z) over time TR, and secondly follows transverse magnetization (M_{XY}) after the application of a 90° pulse for further time TE (*Figure 4*). Contrast between two tissues such as P with a shorter T_1 and T_2, and Q with a longer T_1 and T_2, is shown by the difference in M_{XY} at the time of data collection (dc) at TE as in *Figure 4*.

The voxel signal S for a SE sequence is derived from the simplified Bloch equations so that:

$$S = K\rho_m\left(1-e^{-t/T1}\right)e^{-t/T2} \quad [1]$$

where K is a scaling function, ρ_m is the mobile proton density, and t is time. T_1 and T_2 are time constants. Eq. [1] describes ρ_m in the first segment, recovery of longitudinal magnetization (M_Z) over time in the second segment (which is in parentheses), and decay of transverse magnetization (M_{XY}) over time in the third segment. The equations in the second and third segments are of the forms $y=1-e^{-x}$ and $y=e^{-x}$ respectively.

Eq. [1] describes the signal of a tissue (with specific values of T_1 and T_2) for a SE pulse sequence for specific values of TR and TE. To compare different tissues, at least two curves need to be plotted as in *Figure 4*.

It is useful to replace the variable t in Eq. [1] by the constant times of the SE sequence TR and TE, and to treat the two time constants T_1 and T_2 in Eq. [1] as variables. This changes Eq. [1] to:

$$S = K\rho_m\left(1-e^{-TR/T1}\right)e^{-TE/T2} \quad [2]$$

or:

$$S = KS\rho_m S_{T1}S_{T2} \quad [3]$$

where the signals for the three segments $S\rho_m$, S_{T1} and S_{T2} are given by:

$$S\rho_m = \rho_m, \quad S_{T1} = 1\text{-}e^{-TR/T1}, \quad S_{T2} = e^{-TE/T2} \quad [4]$$

The second and third segments in Eq. [2] are of the forms $y=1-e^{-1/x}$ and $y=e^{-1/x}$ respectively (since T_1 and T_2 are now variables). These forms are quite different from the forms $y=1-e^{-x}$ and $y=e^{-x}$ shown in the second and third segments of the Bloch equations in Eq. [1].

The three segments of Eqs. [2-4] have the features of a linear or exponential filter for ρ_m, [depending on whether the X axis is linear or natural logarithmic (ln)], a low pass filter for T_1 and a high pass filter for T_2 (*Figure 5*).

The signal levels on images are given by Eqs. [2-4] for ρ_m, S_{T1} and S_{T2}, and correspond to the signal or brightness of tissues seen on images.

Eqs. [2-4] can be plotted using a linear or a logarithmic X axis. When using a linear axis, changes in X (i.e., changes in ρ_m, T_1 or T_2) represent absolute differences in TPs. When using a logarithmic X axis, small changes in X (i.e., $\Delta\ln\rho_m$, $\Delta\ln T_1$ and $\Delta\ln T_2$ represent fractional changes in

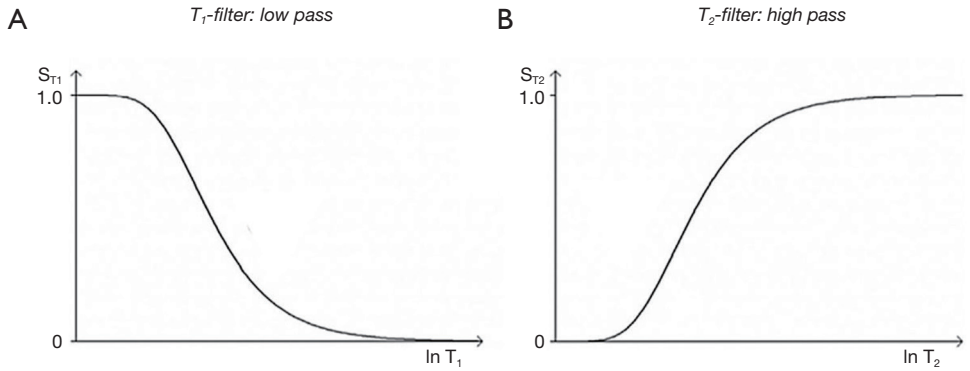

Figure 5 SE T_1 (A) and T_2 (B) TP-filters. Plots of S_{T1} *vs.* ln T_1 (A) and S_{T2} *vs.* ln T_2 (B). The T_1-filter (A) has the appearance of a low pass filter and the T_2-filter (B) has that of a high pass filter. Low values of T_1 "pass" in (A) and high values of T_2 "pass" in (B). SE, spin echo; TP, tissue property.

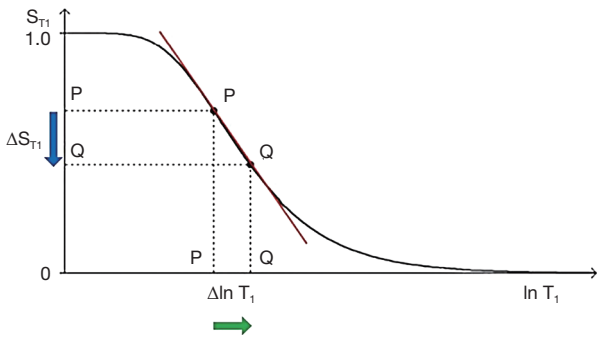

Figure 6 SE sequence. T_1-filter with a ln T_1 X axis. The positive increase in T_1 from P to Q (horizontal green arrow) Δln T_1 is multiplied by the negative slope of the filter (red line) to give negative contrast (vertical blue arrow) $\Delta S_{T1} = C_{ab}$. ΔS_{T1} may be positive or negative. Δln T_1 may also be positive or negative. SE, spin echo.

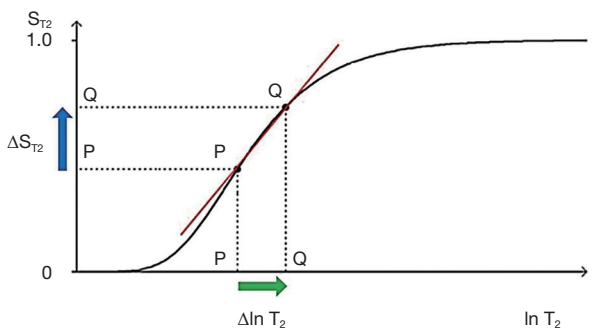

Figure 7 SE sequence. T_2-filter with ln T_2 X axis. The positive increase in T_2 from P to Q (horizontal green arrow) Δln T_2 is multiplied by the positive slope of the filter (red line) to give positive contrast (vertical blue arrow) $\Delta S_{T2} = C_{ab}$. SE, spin echo.

TPs because for small differences between a and b, ln a–ln b = (a–b)/a.

Absolute contrast (C_{ab}) or difference in signal ΔS_{T1} produced by a difference Δln T_1 ($\frac{\Delta T_1}{T_1}$) between the T_1s of two tissues P and Q is shown in *Figure 6* using a ln X axis. A positive change from P to Q of Δln T_1 along the X axis produces a negative change from P to Q along the Y axis, or negative change in signal ΔS_{T1} i.e., contrast $C_{ab}=\Delta S_{T1}$.

The equation for C_{ab} for small changes in ΔT_1 and ΔS_{T1} using a linear X axis is:

$$C_{ab} = \Delta S_{T1} = \frac{\partial ST_1}{\partial T_1} \times \Delta T_1 \quad [5]$$

where $\frac{\partial ST_1}{\partial T_1}$ is the first partial derivative of the T_1-filter with respect to T_1, or the slope of the T_1-filter, x=multiplied, and ΔT_1 is the change in T_1 using a linear X axis.

Using a ln X axis, and noting that $\Delta \ln T_1 = \frac{\Delta T_1}{T_1}$ for small changes in T_1, and that $\frac{dy}{d(\ln x)} = \frac{xdy}{dx}$, where x is a variable, Eq. [5] becomes:

$$C_{ab} = \Delta S_{T1} = \frac{\partial ST_1}{\partial \ln T_1} \times \frac{\Delta T_1}{T_1} \quad [6]$$

where $\frac{\partial ST_1}{\partial \ln T_1}$ is the slope of the filter, or the first partial derivative with respect to lnT_1 (when using a ln X axis), x=multiplied in this and subsequence equations, and $\frac{\Delta T_1}{T_1}$ is the fractional change in T_1 as in *Figure 6*. For the T_1 filter,

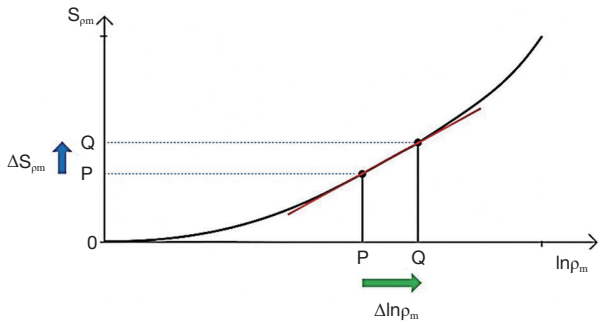

Figure 8 SE sequence. ρ_m-filter with ln ρ_m X axis. The positive increase in ρ_m from P to Q (horizontal green arrow) Δln ρ_m is multiplied by the positive slope of the filter (red line) to give the positive contrast (vertical blue arrow) $\Delta S_{\rho m} = C_{ab}$. SE, spin echo.

positive change from P to Q along the X axis results in negative change from P to Q along the Y axis i.e., negative contrast C_{ab}. The slope of the curve, which is the sequence weighting for the T_1 segment, is negative.

For the T_2 filter (*Figure 7*), positive change $\Delta \ln T_2 = \frac{\Delta T_2}{T_2}$ from P to Q along the X axis results in positive change $\Delta S_{T2} = C_{ab}$ from P to Q along the Y axis i.e., positive contrast. The slope of the filter, which is the sequence weighting for the T_2 segment, is positive.

Solving for the situation when the second derivative of the TP-filter is equal to zero yields the TP value where the slope of the filter, and therefore the contrast, is highest. For the T_1- and T_2-filters, the slope is greatest at TR=T_1 and TE=T_2 when using a ln X axis, and at TR=2T_1 and TE=2T_2 when using a linear X axis.

A similar pattern for contrast applies to ρ_m where an increase in ρ_m and positive slope of the ρ_m-filter produce positive contrast $\Delta S\rho_m = C_{ab}$ (*Figure 8*).

For fractional contrast $C_{fr}=\Delta S/S$ (rather than $C_{ab}=\Delta S$), Eqs. [5,6] are divided by S_{T1} and S_{T2} respectively for non-zero values of S_{T1} and S_{T2}.

So, for T_1 using a ln X axis:

$$C_{fr} = \frac{1}{S_{T1}} \frac{\partial ST_1}{\partial \ln T_1} \times \frac{\Delta T_1}{T_1} \quad [7]$$

and for T_2 using a ln X axis:

$$C_{fr} = \frac{1}{S_{T2}} \frac{\partial ST_2}{\partial \ln T_2} \times \frac{\Delta T_2}{T_2} \quad [8]$$

The filters can be considered separately (i.e., a univariate model for each TP alone, as above), or be combined in a multivariate model. This shows the contributions of the sequence weightings and changes in each TPs to overall contrast for each of ρ_m, T_1 and T_2 in the SE sequence and is illustrated in *Figure 9*.

From Eqs. [3,4] for small change in $\Delta\rho_m$, ΔT_1 and ΔT_2, and using a ln X axis, the product rule from differential calculus gives:

$$\Delta S = \frac{\partial S\rho_m}{\partial \ln \rho_m} S_{T1} S_{T2} \times \frac{\Delta \rho_m}{\rho_m} + S_{\rho m} \frac{\partial ST_1}{\partial \ln T_1} S_{T2} \times \frac{\Delta T_1}{T_1} + S_{\rho m} S_{T1} \frac{\partial ST_2}{\partial \ln T_2} \times \frac{\Delta T_2}{T_2} \quad [9]$$

Normalizing Eq. [9] by dividing it by S and using Eq. [3], for non-zero values of S, $S\rho_m$, S_{T1} and S_{T2}, Cfr is given by:

$$C_{fr} = \frac{\Delta S}{S} = \frac{1}{S\rho_m} \frac{\partial S\rho_m}{\partial \ln \rho_m} \times \frac{\Delta \rho_m}{\rho_m} + \frac{1}{S_{T1}} \frac{\partial T_1}{\partial \ln T_1} \times \frac{\Delta T_1}{T_1} + \frac{1}{S_{T2}} \frac{\partial ST_2}{\partial \ln T_2} \times \frac{\Delta T_2}{T_2} \quad [10]$$

Thus the contributions of the TPs to the overall contrast C_{fr} are for each TP its sequence weighting multiplied by the fractional change in the TP. The relative contributions of each TP to sequence and image weighting can be calculated and expressed as ratios.

From Eq. [10] the overall fractional contrast Cfr using a ln X axis is given by:

$$C_{fr} = \sum_{TP}^{n} \left(\frac{1}{S_{TP}} \frac{\partial S_{TP}}{\partial \ln TP} \times \frac{\Delta TP}{TP} \right) \quad [11]$$

where $\frac{1}{S_{TP}} \frac{\partial S_{TP}}{\partial \ln TP}$ is the sequence weighting for the TP and $\frac{\Delta TP}{TP}$ is the fractional change in the TP. This is one form of the CCT for MRI and its corollaries which are shown in *Figure 10*. Using a ln X axis, the contrast for each TP is the normalized first partial derivative with respect to lnTP multiplied by the fractional change in TP. The total fractional contrast C_{fr} is the algebraic sum of the contributions to contrast from each TP. For T_1 and T_2, if both fractional contrasts are positive, or if both are negative, a synergistic contribution to overall C_{fr} results. If one TP contrast is negative and the other is positive a reduction in overall C_{fr} results. Thus, to achieve synergistic contrast, contributions to contrast of the same sign are sought from each of the relevant TPs to make their effects complementary.

The IR sequence

The IR sequence has an additional T_1-filter (segment) to those of the SE sequence shown in *Figure 9* for which:

$$S_{T1} = \left(1 - 2e^{-T1/T1}\right) \quad [12]$$

This T_1-filter is shown in phase-sensitive (ps)

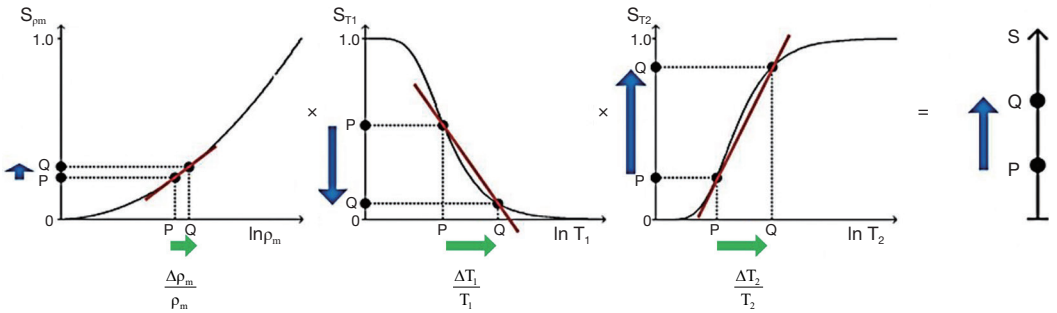

Figure 9 SE sequence with combination of ρ_m, T_1 and T_2-filters. Increases in $\Delta\rho_m/\rho_m$, $\Delta T_1/T_1$ and $\Delta T_2/T_2$ (horizontal green arrows) are multiplied by the slopes of their respective filters (red lines) to produce positive, negative, and positive ρ_m, T_1 and T_2 contrasts from their respective filters (vertical blue arrows with each filter). The overall contrast (blue arrow on right) is the algebraic sum of the TP contrasts produced by each of the three filters (blue arrows with each filter). SE, spin echo; TP, tissue property.

With linear X axis, i.e. TP

$$C_{fr} = \sum_{TP}^{n} \frac{1}{S_{TP}} \frac{\partial S_{TP}}{\partial TP} \cdot \Delta TP$$

With logarithmic X axis, i.e. lnTP

$$C_{fr} = \sum_{TP}^{n} \frac{1}{S_{TP}} \frac{\partial S_{TP}}{\partial \ln TP} \cdot \frac{\Delta TP}{TP}$$

C_{fr} = ΔS/S, fractional contrast

TP = ρ_m, T_1, T_2, T_2*, D*, T_2/T_1.....

S_{TP} = TP-filter for each pulse sequence SE, IR, PGSE, SGE, bSSFP...

$\frac{\partial S_{TP}}{\partial TP}$ = First partial derivative of S_{TP} with respect to TP for linear X axis; is sequence weighting and slope of filter

$\frac{\partial S_{TP}}{\partial \ln TP}$ = First partial derivative of S_{TP} with respect to lnTP for logarithmic X axis; is sequence weighting and slope of filter

ΔTP = Difference or change in TP

$\frac{\Delta TP}{TP}$ = Fractional difference or change in TP

Figure 10 The central contrast theorem for MRI and a corollary. The signal equations for C_{fr} are shown with a linear X axis (TP) (upper) and with a logarithmic X axis (ln TP) (lower). The theorem relates fractional contrast C_{fr} to differences/changes in TPs and provides solutions to the central contrast problem outlined in *Table 1*, i.e., the relationship between the differences/changes in TPs shown in the first column in *Table 1* and differences/changes in signal or contrast shown in the third column of *Table 1*. TP, tissue property.

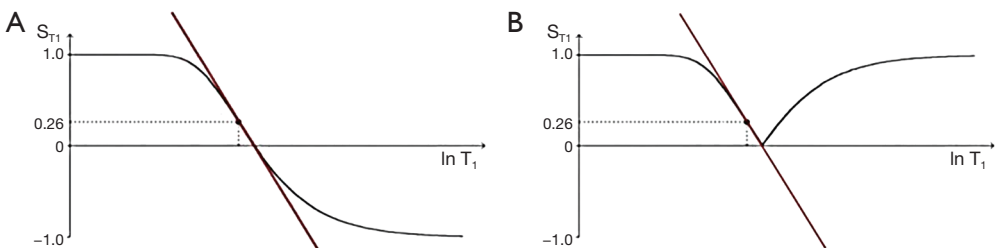

Figure 11 Inversion recovery T_1-filters with phase-sensitive (ps) (A) and magnitude (m) reconstruction (B) using ln T_1 axes. (A) shows both positive and negative values for S_{T1} whereas in (B) negative values are "reflected" across the X axis and become positive. The maximum slopes of the filters are shown as red lines and are negative in both cases.

reconstructed form in *Figure 11A* and in magnitude (m) reconstructed form in *Figure 11B*.

When TI is increased, the T_1-filter shifts to the right as show for the m form in *Figure 12*. *Figure 12A* shows the IR T_1-filter with a short TI_s (e.g., the STIR sequence) for the brain where gray matter (G) has a higher signal than white matter (W). The slope of the filter between W and G is strongly positive. When TI is increased to an intermediate

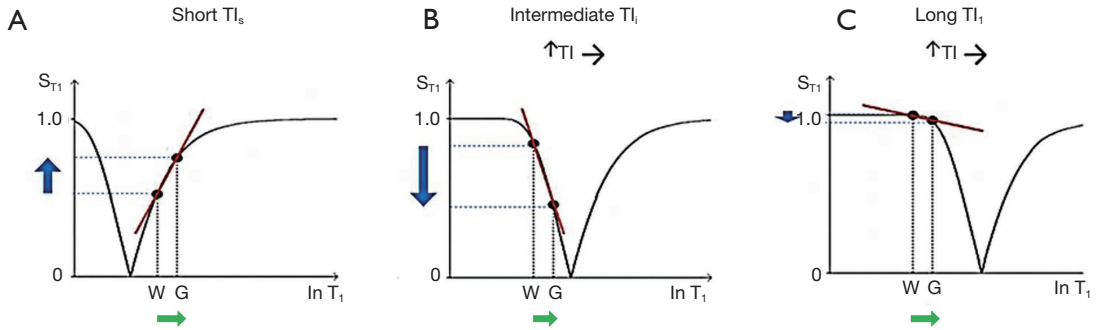

Figure 12 The long TR inversion recovery sequence. T_1-filters for short TI_s (A), intermediate TI_i (B) and long TI_l (C) values. The positions of white (W) and gray (G) matter are the same for each TI. TI is increased from TI_s (left) to TI_i (center) and then further to TI_l (right). The increase in T_1 from W to G (green arrows) is multiplied by the relevant slopes of the filters (red lines) and produces strongly positive, strongly negative, and mildly negative contrast respectively (blue arrows), as TI is increased from left to right.

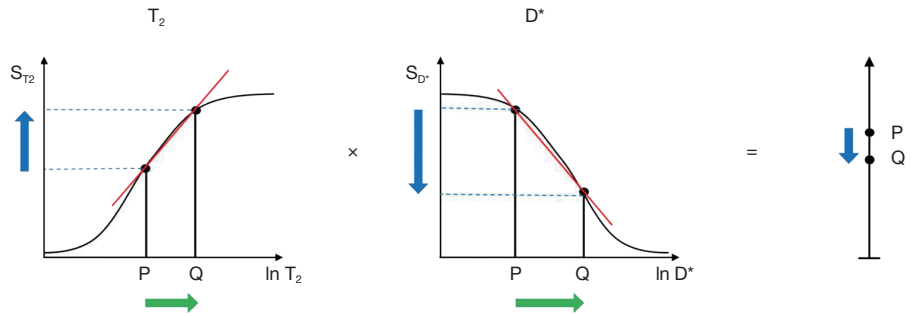

Figure 13 Pulsed gradient spin echo sequence T_2 and D*-filters. Increases in both T_2 and D* from P to Q (positive horizontal green arrows) result in positive and negative contrast respectively, and low opposed negative overall contrast (blue arrow, right).

TI_i as in *Figure 12B* with W and G fixed in the same position on the ln X axis, W now has a higher signal than G. The slope of the filter between them is strongly negative. When TI_i is increased further to a long TI_i as in *Figure 12C*, W is slightly higher signal than G and the slope of the filter between them is negative but of smaller size than in *Figure 12B*. The sequence weighting, which is the slope or first partial derivative of the filter is highly positive in (A), highly negative in (B) and slightly negative in (C) using a short TI_s (A), an intermediate TI_i (B) and a long TI_l (C) respectively. When $TR>>T_1$ with the IR sequence the other T_1 filter ($1-e^{-TR/T1}$) becomes ~1 and the main determinant of contrast is the ($1-2e^{-TI/T1}$) filter.

The pulsed gradient spin echo (PGSE) sequence

For diffusion using the PGSE sequence an additional segment is added to those shown in *Figure 9* for the SE sequence and is illustrated in *Figure 13* under D*. The extra segment is the D*-filter which has the form of an exponential decay with its signal S_{D*} given by:

$$S_{D^*} = e^{-bD^*} \quad [13]$$

b is the diffusion sensitivity parameter and D* is the apparent diffusion coefficient. Significant D*-weighting requires a long TE with the PGSE sequence using present day clinical scanners. This is to provide time for the two pulsed diffusion gradients to be applied before and after the inversion pulse of the SE sequence. The long TE necessary for this creates T_2-weighting and so the sequence simultaneously has positive T_2-weighting (positive slope of the T_2-filter shown in *Figure 13* under T_2), and negative D*-weighting (negative slope of the D*-filter shown in *Figure 13* under D*). Positive change ΔT_2 from P to Q along the X axis (horizontal green arrow) produces positive T_2 contrast (positive vertical blue arrow). Positive change ΔD* from P to Q along the X axis produces negative D* contrast (negative vertical blue arrow). The result of the opposed

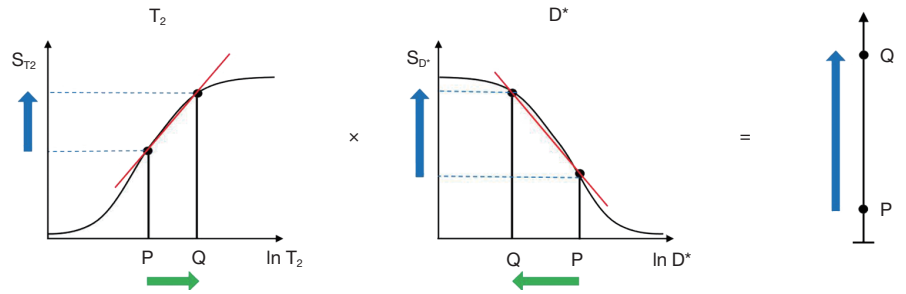

Figure 14 Pulsed gradient spin echo sequence T_2 and D*-filters. Increase in T_2 and decrease in D* from P to Q (positive and negative horizontal green arrows) both produce positive contrast and, as a consequence, high positive overall synergistic contrast (vertical blue arrow, right).

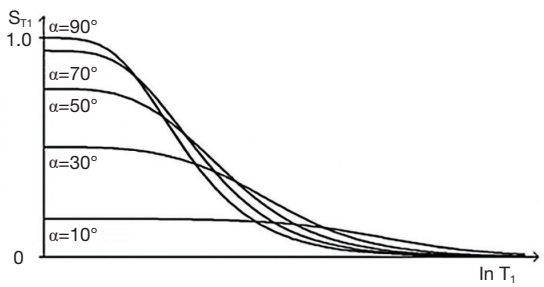

Figure 15 Spoiled gradient echo sequence T_1-filter. For a given TR as a decrease from 90° to 10° the negative slope of the curve (which is its T_1 sequence weighting) generally decreases in size.

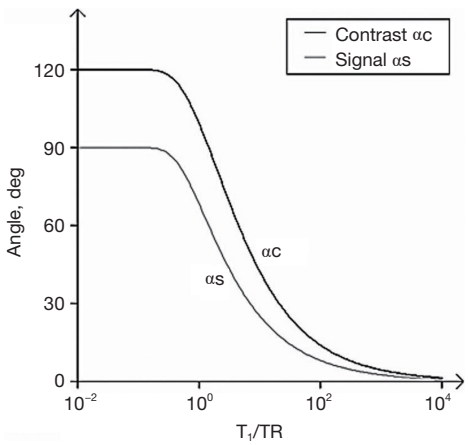

Figure 16 Values of αs and αc. For a given value of the ratio T_1/TR the value of αs to maximize signal can be calculated from Eq. [14] and is shown. The value of αc to maximize absolute contrast for values of T_1/TR is also shown and is greater than αs. It can also be calculated from Eq. [14].

T_2 and D* contrasts produced in this way is overall low negative contrast (negative vertical blue arrow on the right). This is the case in many tissues where disease produces an increase in both T_2 and D*, and the resulting opposed diffusion and T_2 contrasts produce low overall contrast.

Figure 14 shows the situation when T_2 is increased from P to Q under T_2, and D* is decreased from P to Q under D* (rather than increased as in *Figure 13*). The changes in T_2 and D* both result in positive contrast (blue arrows) and the algebraic sum of these is synergistic and produces high positive contrast (vertical blue arrow on right). In this situation, the PGSE T_2 and diffusion weightings work together with the changes in T_2 and D* to produce synergistic contrast.

The spoiled gradient echo (SGE) sequence

The SGE sequence has a T_1-filter which is affected by two pulse sequence parameters TR and the flip angle α {Eq. [14]}. The filter appears the same as the SE sequence for flip angle α=90° but as α is reduced, the curve flattens and there is less T_1 sequence weighting for a given value of TR (*Figure 15*).

$$S = \frac{\sin\alpha}{1-\cos\alpha e^{-\frac{TR}{T_1}}}\left(1-e^{-\frac{TR}{T_1}}\right) \quad [14]$$

S is signal, α is the flip angle, and TR is repetition time. The flip angle to maximize signal αs is determined by setting the first derivative of Eq. [14] to zero. The flip angle to maximize contrast αc is determined by setting the second derivative of Eq. [14] to zero.

Values of αs, to maximize signal and to αc to maximize contrast are shown in *Figure 16* for different values of TR

and T_1.

With the SGE sequence, the T_2-filter of the SE sequence becomes a T_2*-filter and includes additional effects from susceptibility which make T_2* less than T_2, and chemical shift. Chemical shift effects are modelled by including phase differences for water and fat and taking the vector sum and difference of these as with the Dixon technique.

Features of TP-filters

Features of the TP-filters approach include:

(i) Placement of TPs along the X axis, and the use of both ln and linear scales along this axis.
(ii) Placement of signal S, or Q along the Y axis and use of both linear and logarithmic scales for this.
(iii) Use of both absolute contrast C_{ab} and fractional contrast C_{fr}.
(iv) Designation of the slope or first derivative of the TP-filter (or normalized slope of the TP-filter) as sequence weighting and calculation of this slope both for linear and ln X axes.
(v) The use of second derivatives of the TP-filter and points of inflection to calculate values of sequence parameters (e.g., TR=T_1, TE=T_2 with ln X axes) to maximize C_{ab}.
(vi) Allocation of signs (positive or negative) to each of signal, contrast, image weighting, sequence weighting and TP differences/changes. This makes it possible to understand contrast and weighting in semi-quantitative and quantitative terms.
(vii) Separation of sequence and image weighting with calculation of sequence and image weighting ratios to determine the relative contributions of different TPs to sequence weighting and image weighting.
(viii) Ability to deal with the situation where a single TP (e.g., T_1) is affected by two pulse sequence parameters (TR, a), or a single pulse sequence parameter (e.g., TE) has effects on two TPs (e.g., T_2 and D*).
(ix) TP values cover the full extent experienced in clinical practice so the graphics provide a complete representation of the contrast and weighting that is seen on images.
(x) The same approach can be used for sequence preparations as well as complete pulse sequences.
(xi) Although developed here primarily for ρ_m, T_1, T_2, D* and T_2*. The TP-filters approach is also applicable to other TPs.

Features of the CCT and its corollaries

First and foremost, unlike conventional qualitative weighting which only utilizes a single tissue TP to explain contrast, the CCT makes it possible to deal with two or more TPs and understand their separate and combined contributions to contrast. As a result, use of the CCT resolves many of the inconsistencies associated with the use of conventional qualitative weighting. Resolution of one of these inconsistencies is shown in *Figure 17* which explains the fact that a SE sequence which is T_1-weighted for the brain is T_2-weighted for disease in the Achilles tendon, as was illustrated in *Figure 3*. It also makes it possible to understand how T_2 and D* contrast behave individually and how they interact with each other in the PGSE sequence (*Figures 13*,*14*).

The CCT formalizes the relationship between differences/changes in TPs and fractional contrast, C_{fr} (*Figure 10*). It is in two parts. Firstly, for each TP the fractional contrast generated is the normalized product of sequence weighting (partial derivative of the TP-filter either with respect to the TP or lnTP) multiplied by the change in TP, or the fractional change in TP. The second part is the algebraic sum of the fractional contrasts generated by each TP which is the overall fractional contrast C_{fr}. For signal S, the CCT and its corollaries are derived from the Bloch equations for ρ_m, T_1 and T_2 and the Torrey equations which add diffusion D*. The CCT is used in graphical form in this paper.

The CCT can be used in qualitative form to determine which single TP of several is most responsible for contrast for given changes in the TPs and a specific pulse sequence. It is the TP with the largest C_{fr}. It can also be used in semi-quantitative or graphical form where the sign of differences/changes in TP and their relative magnitudes are considered. It can also be used in quantitative form where sequence and image weighting ratios express in percentages the relative contributions of each TP to sequence weighting and to image weighting using the equations:

$$sW^r\left(\rho_m:T_1:T_2\right)=\left(\frac{1}{S\rho_m}\frac{S\rho_m}{\partial\ln\rho_m}:\frac{1}{S_{T1}}\frac{\partial ST_1}{\partial\ln T_1}:\frac{1}{S_{T2}}\frac{\partial ST_2}{\partial\ln T_2}\right) \quad [15]$$

$$iW^r\left(\rho_m:T_1:T_2\right)=\left(\frac{1}{S\rho_m}\frac{\partial S\rho_m}{\partial\ln\rho_m}\cdot\frac{\Delta\rho_m}{\rho_m}:\frac{1}{S_{T1}}\frac{\partial ST_1}{\partial\ln T_1}\cdot\frac{\Delta T_1}{T_1}:\frac{1}{S_{T2}}\frac{\partial ST_2}{\partial\ln T_2}\cdot\frac{\Delta T_2}{T_2}\right) \quad [16]$$

The sequence weighting ratio sW^r describes the relative weighting of the TPs within a sequence. The image weighting ratio (iW^r) uses the sequence weighting ratio and combines it with differences/changes in each TP to describe their relative effects on the contrast of the image. This is an

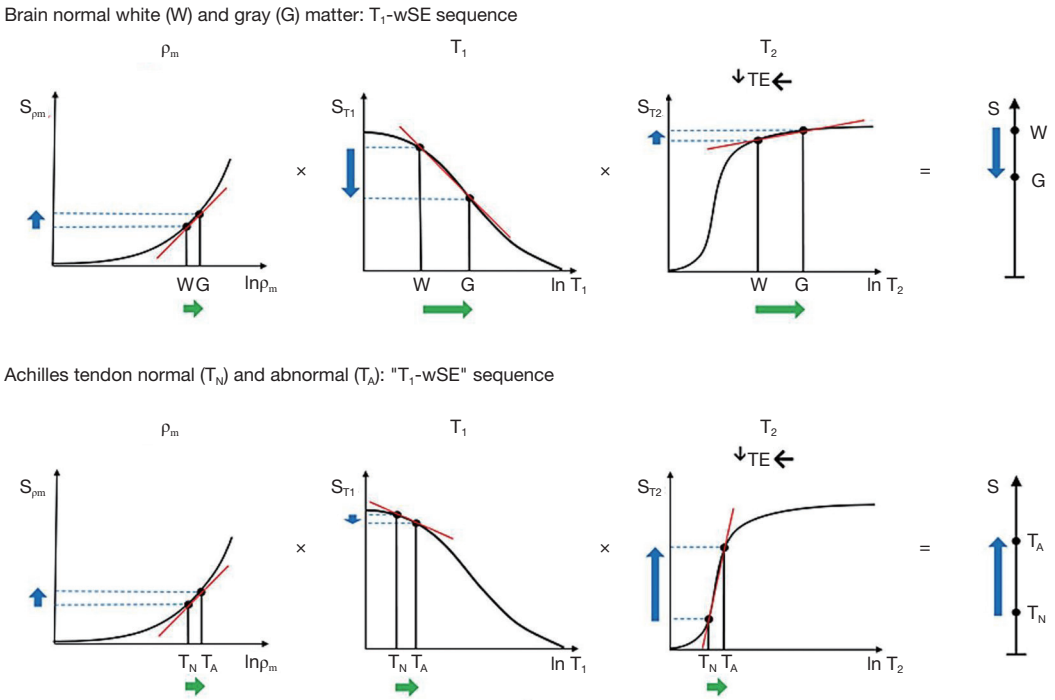

Figure 17 Normal white (W) and gray (G) matter in the brain (upper), as well as normal (T_N) and abnormal (T_A) Achilles tendon (lower) imaged with the same T_1-wSE sequence. The T_1-wSE sequence ρ_m, T_1 and T_2 TP-filters are the same in the upper and lower figures. In the upper figure ρ_m, T_1 and T_2 are increased from W to G matter. The TP sequence weightings are the slopes of filters (red lines) which are positive for ρ_m, negative for T_1 and positive for T_2. The contrast produced by each filter is the increase in each TP (horizontal green arrows) multiplied by the slope of the relevant TP-filter (red lines) and these are shown as vertical blue arrows for each filter. They are slightly positive for ρ_m, markedly negative for T_1 and slightly positive for T_2 (upper). The overall fractional contrast is the algebraic sum of the fractional contrasts for each TP. This is shown as the vertical blue arrow (right side) and is negative (upper). In the lower part of the figure, the normal T_1 of the Achilles tendon is shorter than that of W matter (upper) and corresponds with a flatter negative part of the T_1-filter (lower). The normal T_2 of the Achilles tendon (lower) is shorter than that of W matter (upper) and corresponds with a steeply positive sloping part of the T_2-filter (lower). The abnormality in the Achilles tendon shows an increase in ρ_m, T_1 and T_2 (green arrows) (lower). These changes are multiplied by the positive ρ_m, slightly negative T_1 and highly positive slopes of the ρ_m, T_1 and T_2-filters respectively (red lines). These give positive, slightly negative and strongly positive TP contrasts respectively (vertical blue arrows for each filter). The overall fractional contrast, which is the algebraic sum of the fractional TP contrasts, is highly positive (right side, blue vertical arrow) (lower). Because of the shorter T_1 and T_2 of the Achilles tendon relative to the T_1 and T_2 of W and G matter, there is a shift from the dominant negative T_1-weighting and contrast for W relative to G (i.e., steeper T_1 and flatter T_2 in the corresponding parts of the T_1 and T_2-filters) (upper), to the dominant positive T_2-weighting and contrast for the change from normal (T_N) to abnormal (T_A) in the Achilles tendon (flatter T_1 and steeper T_2 in the corresponding parts of the T_1 and T_2-filters) (lower). The designation "T_1-weighted" is usually applied to the "T_1-wSE" sequence when it is used for the Achilles tendon even though the sequence and contrast are both actually T_2-weighted. This may be because there is already a long TR long TE T_2-weighted SE sequence in regular use in the musculoskeletal system, and re-designating the "T_1-wSE" sequence as T_2-weighted as well could cause confusion.

important difference. The sequence T_1-filter may be steeper than its T_2-filter meaning that it is more T_1-weighted than it is T_2-weighted for particular values of T_1 and T_2. However, if disease results in a larger change in T_2 than in T_1, contrast on the image can be dominated by the T_2 change not the T_1 change, so that the image has a dominant T_2-weighting in spite of the fact that the sequence has a dominant T_1-weighting.

The CCT and its corollaries employ the small change approximation of differential calculus. This is applicable, in particular, to the detection of effects due to small changes in TPs which is appropriate for demonstration of subtle

Table 2 MASDIR sequences

Groups of MASDIR sequences	Expansion of MASDIR sequence acronyms
MIR	**Multiplied IR**
DIR	Double IR ($mTI_i \times mTI_{s/i}$)
MP2RAGE	Magnetization Prepared 2 Rapid Acquisition Gradient Echo ($psTI_i \times psTI_i$) (also added and divided)
AIR	**Added IR**
AIR	Added IR ($mTI_{s/i/l} + mTI_{s/i/l}$)
A^1IR	Added IR ($psTI_{s/i/l} + mTI_{s/i/l}$)
A^1IRES	AIR Added IR Echo Subtraction
S^1AIR	Subtracted, Added IR
SIR	**Subtracted IR**
SIR, rSIR	Subtracted IR ($mTI_{s/i/l} - mTI_{s/i/l}$), reverse SIR
SIRES, rSIRES	Subtracted IR Echo Subtraction, reverse SIRES
SIREDS, rSIREDS	Subtracted IR Echo Diffusion Subtraction, reverse SIREDS
SIRGES, rSIRGES	Subtraction IR Gradient Echo Subtraction, reverse SIRGES
SIRDGES, rSIRDGES	Subtraction IR Diffusion and Gradient Echo Subtraction, reverse SIRDGES
*DESIRE, STAIRES	Double Echo Sliding IR, Short TR Adiabatic pulse prepared IR (TR x $mTI_{i/s}$) Echo Subtraction
*shMOLLI	Shortened Modified Look-Locker Inversion Recovery
S^1IR	Subtracted IR ($psTI_{s/i/l} - mTI_{s/i/l}$)
S^2IR	Subtracted SIR
IRES	IR Echo Subtraction
STIRES	Short TI IR Echo Subtraction
dIR	**Divided IR**
dSIR, drSIR	Divided SIR, divided reverse SIR
dSIRES, drSIRES	Divided SIRES, divided reverse SIRES
dSIREDS, drSIREDS	Divided SIREDS, divided reverse SIREDS
dSIRGES, drSIRGES	Divided SIRGES, divided reverse SIRGES
dSIRDGES, drSIRDGES	Divided SIRDGES, divided reverse SIRDGES
FLAWS div	Fluid and white matter suppressed, divided
FLAWS hc, FLAWS hco	FLAWS high contrast, FLAWS high contrast opposed
FIR	**Fitted IR (multiple TIs)**
MPnRAGE	Magnetization Prepared Rapid Acquisition Gradient Echo
*shMOLLI	Shortened Modified Look-Locker Inversion Recovery
*DESIRE	Double Echo Sliding IR

*, included in both the subtracted and fitted categories. MASDIR, multiplied, added, subtracted and/or divided inversion recovery.

disease. When large changes are present the small change approximation may lead to errors, but this is a known issue and is usually not a problem in clinical practice since large changes are usually easy to detect.

The use of fractional contrast involves normalization by the TP filter signals S_{TP} as well as the overall signal S. If one or more of these is zero, or close to zero when image noise is taken into account, values may take the form 1/0 and be uninterpretable. It means that fractional contrast is only valid between certain limits.

It is also not obvious which of absolute contrast C_{ab} or fractional contrast C_{fr} best represent what is visually perceived by human observers and therefore provides the more appropriate model for understanding contrast. As a result, in this paper consideration is given to both forms of contrast.

The signal and contrast produced by sequences are subject to changes in window width and level performed by the observer. This has an effect on the perception of contrast and also needs consideration.

MASDIR pulse sequences

Development of the MASDIR sequence

The first combination of two IR sequences to form a single sequence was described in 1985 (6). This was the use of two successive inversion pulses to suppress signal from fluid then fat and was applied in the brain and body as the Double IR (DIR) sequence. Its use was extended to suppression of either white or gray matter signals as well as CSF in 1994 (7). More recently, in 2010 the Magnetization Prepared 2 Rapid Acquisition Gradient Echo (MP2RAGE) sequence was described (8). It multiplies two IR sequences together and normalizes them.

Groups of MASDIR sequences

A classification of MASDIR sequences is shown in *Table 2*. They are divided into: (i) multiplied, (ii) added, (iii) subtracted, and (iv) divided. Fitted IR (FIR) sequences are treated as a separate category. There are many types of MASDIR sequences and these are discussed briefly below. Subsequent sections describe some of them in more detail.

Multiplied IR (MIR) sequences

MIR sequences include DIR and MP2RAGE as mentioned above.

Added IR (AIR and A^1IR) sequences

One group of AIR sequences adds two magnitude reconstructed sequences with different TIs and is used with subtraction and division (see below). Another group of sequences (A^1IR) use a single TI with images reconstructed in ps and m forms. Addition of these two sequences shows shorter T_1 tissues and suppresses the signal from longer T_1 tissues and fluids. The A^1IRES sequence supplements this by Echo Subtraction (ES, see later) and so adds a T_2-filter reducing the signal from longer T_2 tissues and fluids to provide a combined short T_1 short T_2-filter. The Subtracted AIR (S^1AIR) sequence subtracts a longer TI image from a shorter one to selectively show a specific range of short T_1 tissues.

SIR sequences

Eight subgroups of SIR sequences are included in *Table 2*. The first five use subtraction of a longer TI image from a shorter TI one (or vice versa as the reversed or r form). They start with the basic sequence (SIR), add T_2-weighting to it as the SIRES sequence, and then add D*-weighting to this as the SIREDS sequence. The SE segment of the SIRES sequence is substituted by a gradient echo to produce the SIRGES sequence. This can have added to it diffusion weighting as the SIRDGES sequence.

The sixth group includes Double Echo Sliding Inversion REcovery (DESIRE) (9) which uses a sliding TI window to obtain many IR images with different TIs followed by a UTE data collection (dc) and ES, and the Short TR Adiabatic IR Echo Subtraction (STAIRES) (10) sequence. This sequence multiplies a very short TR segment by a short intermediate TI_s segment to reduce to zero, or nearly zero, long T_1 and T_2 signals from tissues with a wide range of T_1s. It is used with UTE dcs to provide selective imaging of ultrashort T_2 tissues. This is followed by ES to reduce to zero the signal from any long T_2 tissues which are not completely nulled. Both the DESIRE and STAIRES sequences can be used selectively to image myelin and other ultrashort T_2 tissues.

The seventh group uses the same TI and subtracts a ps image from a m image once (S^1IR), or twice (S^2IR) with different TIs, for example, to selectively show a fluid or tissue.

The eighth group of SIR sequences is a basic IR Echo Subtraction (IRES), and the STIRES (STIR and ES) sequence which nulls shorter T_1 white adipose tissue (WAT) and uses Dixon subtraction of out-of-phase images from in-phase images to selectively show lipid present in BAT as a result of its longer T_1 compared to the T_1 of lipid in WAT.

Divided IR (dIR) sequences

A central issue with division of IR sequences is the behaviour of the filter if or when the denominator takes a value of zero. This potentially leads to infinite values of the filter. Even if zero values are avoided, there are values when the denominator approaches zero and division becomes unreliable as a result of noise and artifacts.

The problem can largely be avoided with two SIR images by making the denominator the addition of the signals in the two images. The filters have different TIs, and using magnitude reconstruction, the sum of them in the denominator is non-zero. Division also normalizes the sequence so that the effects of ρ_m and T_2 are reduced or eliminated, as are those due to receiver coil inhomogeneity.

Inclusion of division is the main advance over the previous formulation of MASTIR (Multiplied, Added, Subtracted and/or fiTted IR) sequences which are now described as MASDIR sequences. This includes each of the four basic operations of arithmetic and regards the fitted category (i.e., the Fitted IR, FIR sequences) as a separate mathematical operation.

Subtracted (SIR), Added (AIR) and Divided (dSIR) filters (univariate T_1 models)

Two IR filters with different TIs are shown in *Figure 18A*. They are subtracted to give the SIR filter in *Figure 18B*. This T_1-filter is steep in the X axis region between the inversion times, i.e., the middle Domain (mD). The two sequences in *Figure 18A* can also be added as the AIR sequence which is shown in *Figure 18C* where there are higher signal and higher slopes outside of the mD. The mD in *Figure 18C* has a low signal with a nearly linear slightly downward sloping curve.

Figure 19A shows the T_1-filter for the divided Subtracted IR (dSIR) filter in which the SIR filter in *Figure 18B* is divided by the AIR filter in *Figure 18C*. The dSIR filter shows a very highly sloping positive mD.

Figure 19B compares the contrast from the short TI T_1-filter, S_{TIs} (pink) which is that of a conventional intermediate TI_i IR sequence such as magnetization prepared rapid acquisition gradient echo (MP-RAGE) to that from the SIR filter (blue). The vertical pink and blue arrows on the right show that the contrast produced by the SIR filter is about double that produced by the S_{TIs} filter for the same change in T_1 (horizontal green arrow across the mD).

Figure 19C compares the contrast produced by the short

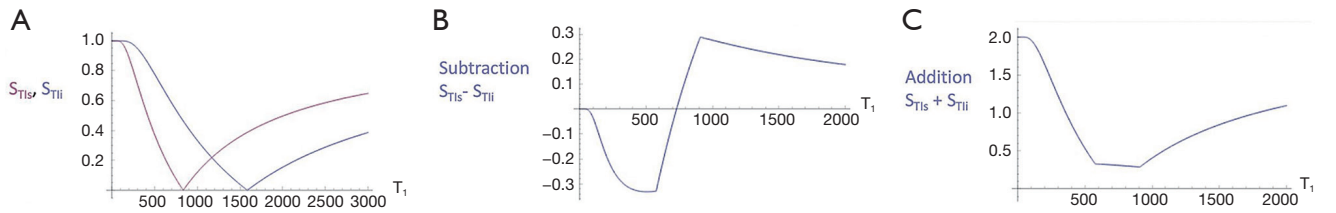

Figure 18 SIR and AIR filters. T_1 is shown along the X axis. (A) shows the TI_s filter (pink) and TI_i filter (blue), (B) shows the subtraction (S_{TIs} - S_{TIi}) IR or SIR filter, and (C) shows the addition (S_{TIs} + S_{TIi}) IR or AIR filter. In (B) the slope of the curve in the mD is nearly double that of the S_{TIs} filter [pink in (A)]. In (C) the signal at T_1=0 is doubled to 2.0, and the signal in the mD is reduced to about 0.35–0.33 in the nearly linear, slightly downward sloping central part of the AIR filter (i.e., the middle Domain, mD). SIR, subtracted inversion recovery; AIR, added inversion recovery.

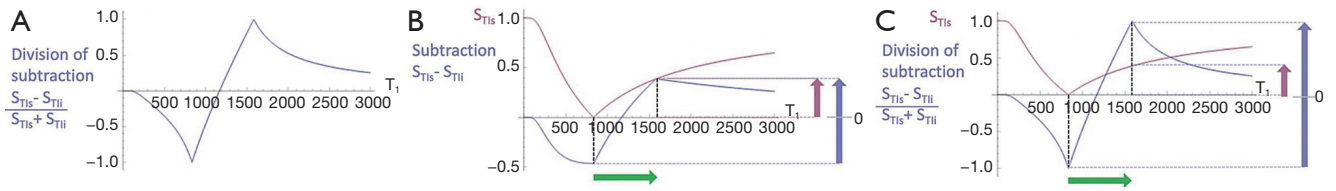

Figure 19 dSIR filter and comparisons of the S_{TIs} filter with the SIR filter, and of the S_{TIs} filter with the dSIR filter for an increase in T_1 in the mD. (A) shows division (d) of the subtraction (S_{TIs}–S_{TIi}) filter by the addition (S_{TIs}+S_{TIi}) filter to give (S_{TIs}–S_{TIi})/(S_{TIs}+S_{TIi}) or SIR/AIR=dSIR filter. (B) shows a comparison of the S_{TIs} filter (pink) and the subtraction SIR filter (blue). (C) is a comparison of the S_{TIs} filter (pink) with the divided subtraction dSIR filter (blue). The dSIR filter in (A) and (C) has maximum and minimum values of 1 and -1 respectively and is steeply sloping. In (B), the increase in signal (i.e., contrast) for the increase in T_1 extending from one end of the mD to the other, for example from white to gray matter (horizontal green arrow) is about 0.35 for the S_{TIs} filter and about 0.75 for the subtraction (SIR) filter. This represents an increase in contrast for the SIR filter compared to the S_{TIs} filter of about two (right vertical arrows). In (C) the change in the S_{TIs} filter is about 0.35 as shown also in (B), and that in the divided subtraction dSIR filter is 2.0 representing an increase in contrast of about five times (right vertical arrows). SIR, subtraction inversion recovery; dSIR, divided SIR; AIR, added inversion recovery.

TI filter, S_{TIs} (pink) to that from the dSIR sequence (blue). For the same change in T_1 (positive horizontal green arrow across the mD) the dSIR filter generates about five times the contrast produced by the S_{TIs} filter (vertical pink and blue arrows). As the second TI is moved closer to the first TI, the slope of the T_1 tissue filter in the mD becomes steeper, and so the T_1 dependent contrast in the mD increases. This is documented in *Table 3*. In this table, as ΔTI decreases from 90% to 13% the ratio of the contrast produced by the dSIR sequence to that produced by the conventional IR sequence increases from 5 to 20. The trade-off for this amplified contrast is a decreased mD where the sequence weighting and the contrast ratio is high. The mathematical basis for this is described in Appendix 1.

Figure 20A illustrates the rSIR filter and shows the same two filters for S_{TIs} and S_{TIi} as in *Figure 18A*. In *Figure 20B* the reverse (r) subtraction rSIR filter is shown. This has a negative slope in the mD. In *Figure 20C* addition of the two original filters gives the AIR filter as shown. *Figure 21A* shows the rSIR filter in *Figure 20B* divided by the AIR filter in *Figure 20C* to give the drSIR filter. This has a steeply sloping negative mD. *Figure 21B* shows a comparison of the S_{TIi} filter (pink) with the rSIR filter (blue) for a decrease in T_1 (negative horizontal green arrow). The contrast produced by the rSIR filter is about twice that of the S_{TIi} filter (vertical pink and blue arrows on right). *Figure 21C* shows a comparison of the S_{TIi} filter (pink) with the drSIR filter (blue). The contrast produced by the drSIR filter is about five times greater than that from the S_{TIi} filter (pink and blue arrows on the right) as a result of using T_1 synergistically to produce contrast 3–4 times.

The image processing for the sequences is shown in *Table 4* for positive change in T_1 (#1) and a negative change in T_1 (#2). The two filters are processed in the same way. The SIR filter gives positive contrast in #1 and negative contrast in #2. The rSIR filter gives negative contrast in #1 and positive

Table 3 TI_s, TI_i, ΔTI, S_{TIs} contrast at TI_i, S_{dSIR} contrast at TI_i, and ratio of S_{dSIR}/S_{TIs} contrast

TI_s (ms)	TI_i (ms)	ΔTI		S_{TIs} contrast	S_{dSIR} contrast	Ratio of S_{dSIR}/S_{TIs} contrast
		ms	%			
580	1,100	520	90	0.40	2.0	5
580	840	260	45	0.25	2.0	8
580	710	130	22	0.15	2.0	13
580	655	75	13	0.10	2.0	20

As TI_i is reduced the mD narrows, ΔTI decreases and the signal for TI_s at TI_i (S_{TIs} value) decreases. The ratio of the dSIR contrast to the S_{TIs} contrast increases from 5 to 20, as ΔTI decreases from 90% to 13% when the mD narrows. dSIR, divided subtracted IR.

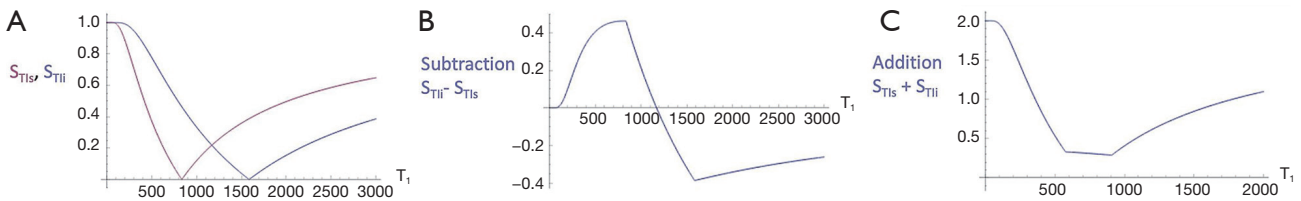

Figure 20 rSIR and AIR filters. T_1 is shown along the X axis. (A) shows the TI_s (pink) and TI_i (blue) filters, (B) shows the subtraction (S_{TIi} -S_{TIs}) or reversed SIR, rSIR filter, and (C) shows the addition (S_{TIs} + S_{TIi}) or AIR filter. In (B) the slope of the filter in the mD is negative and nearly double that of the S_{TIi} filter. In (C) the signal at T_1=0 is doubled to 2.0, and the signal in the mD it is reduced to about 0.38–0.36 as shown in the nearly linear slightly downward sloping central part of the AIR filter (i.e., the mD). rSIR, reverse subtraction inversion recovery; AIR, added inversion recovery.

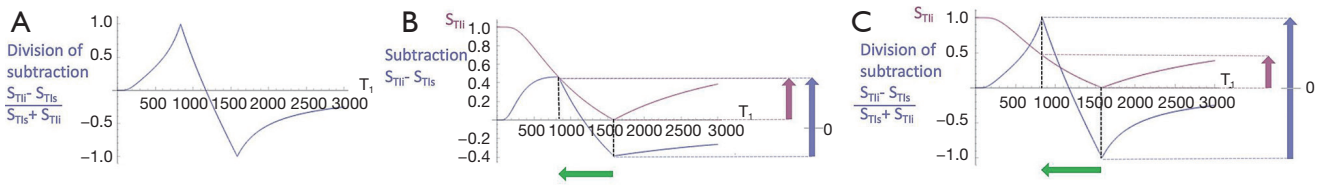

Figure 21 rSIR filter and comparisons of the S_{TIi} filter with the SIR filter, and of the S_{TIi} filter with the drSIR filter for a decrease in T_1 in the mD. T_1 is along the X axis. (A) shows division (d) of the subtraction rSIR (S_{TIi}–S_{TIs}) filter by the AIR filter to give (S_{TIs}–S_{TIi})/(S_{TIs}+S_{TIi}) or rSIR/AIR=drSIR filter. (B) shows a comparison of the S_{TIi} filter (pink) and the reverse subtraction rSIR filter (blue). (C) shows a comparison of the S_{TIi} filter (pink) with the divided subtraction drSIR filter (blue). The drSIR filter in (A) and (C) has maximum and minimum values of 1 and -1 respectively and is steeply sloping. In (B), the increase in signal (i.e., contrast) for the decrease in T_1 from one end of the mD to the other (negative horizontal green arrow) is about 0.38–0.36 for the S_{TIi} filter and about 0.85 for the rSIR filter (vertical blue arrow). This represents an increase in contrast for the rSIR filter compared with the S_{TIs} filter of nearly two (right vertical pink and blue arrows). In (C) the change in the S_{TIi} filter for the same decrease in T_1 is about 0.38–0.36 as in (B) (vertical pink arrow), and that with the divided subtraction drSIR filter is 2.0 (vertical blue arrow) representing an increase in contrast of about five times. rSIR, reverse subtraction inversion recovery; drSIR, divided reverse SIR; AIR, added inversion recovery.

contrast in #2.

The mathematical basis for key features of the dSIR and drSIR filters including their near linearity, slope approximately equal to +/– ln 4/ΔTI and high sensitivity to small changes in T_1 is included in the Appendix 1.

Including T_2 and D*: Subtracted, Added and Divided IR sequences (multivariate models)

Division has also been incorporated as an option using AIR filters in the denominator to give dSIRES, dSIREDS, dSIRGES and dSIRDGES filters as well as their reversed (r)

Table 4 SIR and rSIR sequences image processing

#	Sign of ΔT_1	Image processing	Examples
1	+	Row I (TI_s): (Row I minus Row II) to give SIR, then r; (Row II minus Row I) to give rSIR, then ± d Row II (TI_i)	Many diseases
2	–	Row I (TI_s): (Row I minus Row II) to give SIR, then r; (Row II minus Row I) to give rSIR, then ± d Row II (TI_i)	Some hemorrhage, iron deposition, GBCA/MIOP accumulation

Changes in ΔTP (ΔT_1) in disease can be negative (–) or positive (+). In most diseases, T_1 is increased (+), but in hemorrhage, iron deposition and other diseases T_1 is decreased (–). Image processing in #1 i.e., the subtraction (Row I minus Row II) produces positive T_1 synergistic contrast with SIR processing, and negative T_1 synergistic contrast with reversed rSIR processing. Image processing in #2 produces positive and negative T_1 synergistic contrast with rSIR and SIR processing respectively. SIR, subtraction inversion revovery; rSIR, reverse SIR; d, division; GBCA, gadolinium based contrast agents; MIOP, magnetic iron oxide particles.

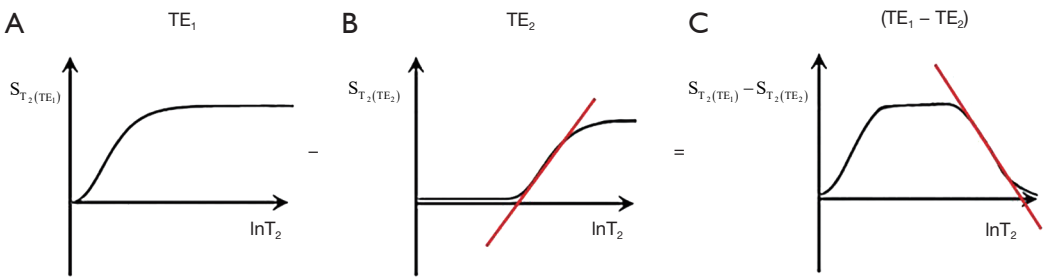

Figure 22 Echo subtraction. Short TE_1, long TE_2 and subtracted (TE_1-TE_2) filters. The positive slope of the TE_2 filter (red line) becomes negative with the (TE_1-TE_2) filter (red line).

forms.

In order to create sequences with synergistic contrast, it is sometimes necessary to reverse the weighting of a conventional filter. ES is used to reverse the T_2-weighting of the T_2-filter. This is accomplished by the subtraction: short TE filter minus long TE filter as in *Figure 22*. Increases in T_2 in the chosen domain for the T_2-filter result in increased signal. For the ES filter, increase in T_2 results in decreased signal. Thus, the T_2-filter weighting has changed from positive to negative.

Row I of *Figure 23* describes a filter with a short TI and a long TE resulting in positive contrast from the T_1 and T_2-filters [middle and right columns (B) and (C)]. Row II of *Figure 23* shows an intermediate TI filter with negative contrast from both the T_1 and T_2-filters. Row II includes the subtraction: intermediate TIi short TE sequence minus intermediate TI_i long TE sequence. Thus, ES reverses the sign of the conventional T_2 filter. In Row III, the SIRES filter is created by the subtraction: Row I minus Row II which produces overall synergistic positive T_1 and T_2 contrast. Row IV shows the reversed subtraction rSIRES. Row V shows the divided dSIRES and drSIRES filters which result in further increase in T_1 contrast as discussed previously.

Diffusion subtraction (DS) is used to reverse the weighting of the D* tissue filter. This is accomplished by the subtraction: D*-filter with b="0" minus D*-filter with a high b value as in *Figure 24*. For the short TE and b="0" filter in *Figure 24A*, increase in D* results in no change. For the diffusion filter in *Figure 24B*, increase in D* results in negative contrast. For the subtracted D*-filter, increase in D* produces positive contrast.

The SIREDS filter (*Figure 25*) adds D* to the SIRES filter and includes DS to create synergistic T_1, T_2 and D* contrast. Row I in *Figure 25* is a filter with a short TIs, long TE, and high b value resulting in positive synergistic contrast for increases in T_1 and T_2, and a decrease in D* as seen in some acute disease and many tumors. Row II in

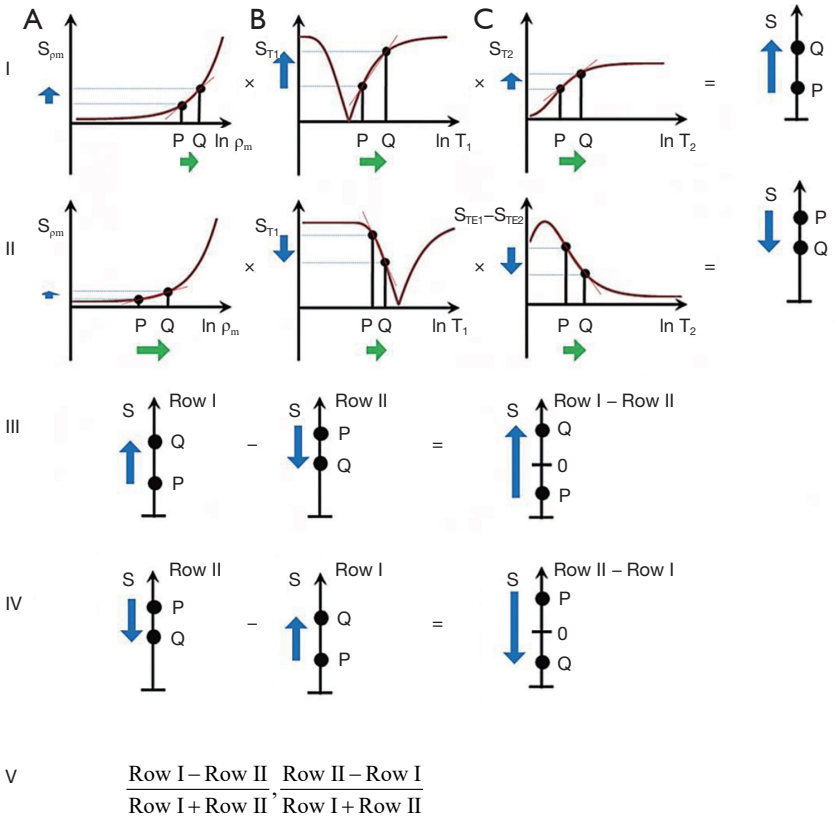

Figure 23 SIRES sequence. Row I shows that increases in ρ_m, T_1 and T_2 (green arrows) produce synergistic positive contrast (blue arrows). Row II (which includes ES) shows that increases in T_1 and T_2 produce synergistic negative contrast. In Row III, the subtraction (Row I minus Row II) results in synergistic positive contrast. In Row IV the reverse subtraction rSIRES produces negative synergistic contrast. Row V shows the divided forms of the sequence dSIRES and drSIRES which have increased T_1 contrast. SIRES, subtracted IR echo subtraction; ES, echo subtraction; rSIRES, reverse SIRES; dSIRES, divided SIRES; drSIRES, divided reversed SIRES.

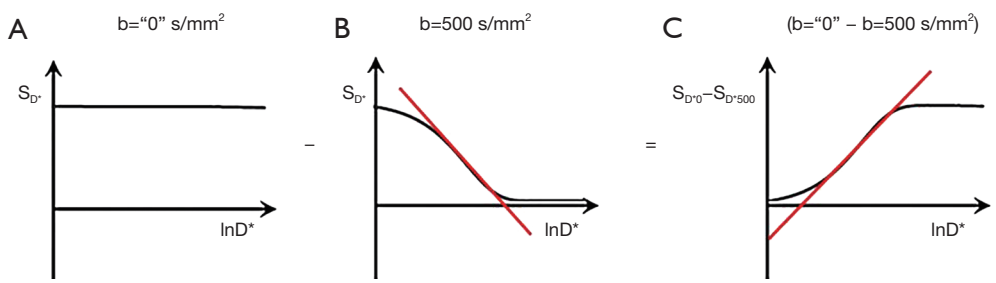

Figure 24 Diffusion subtraction. b="0" s/mm^2 (A), b=500 s/mm^2 (B) and subtracted (b="0" – b=500 s/mm^2) (C) filters. The negative sequence weighting in (B) becomes positive in (C) (red lines).

Figure 25 is a filter with negative synergistic contrast for increase in T_1 and T_2 and decrease in D*. Row II includes the subtraction: intermediate TI_i, short TE, b="0" filter minus intermediate TI_i, short TE, high b value [i.e., ES and diffusion subtraction (EDS)]. Row III shows the subtraction: Row I minus Row II to give the SIREDS filter. Row IV shows the rSIREDS filter. The dSIREDS and drSIREDS filters are shown in Row V and increase T_1-weighting as above.

The Fluid and White Matter Suppressed (FLAWS)

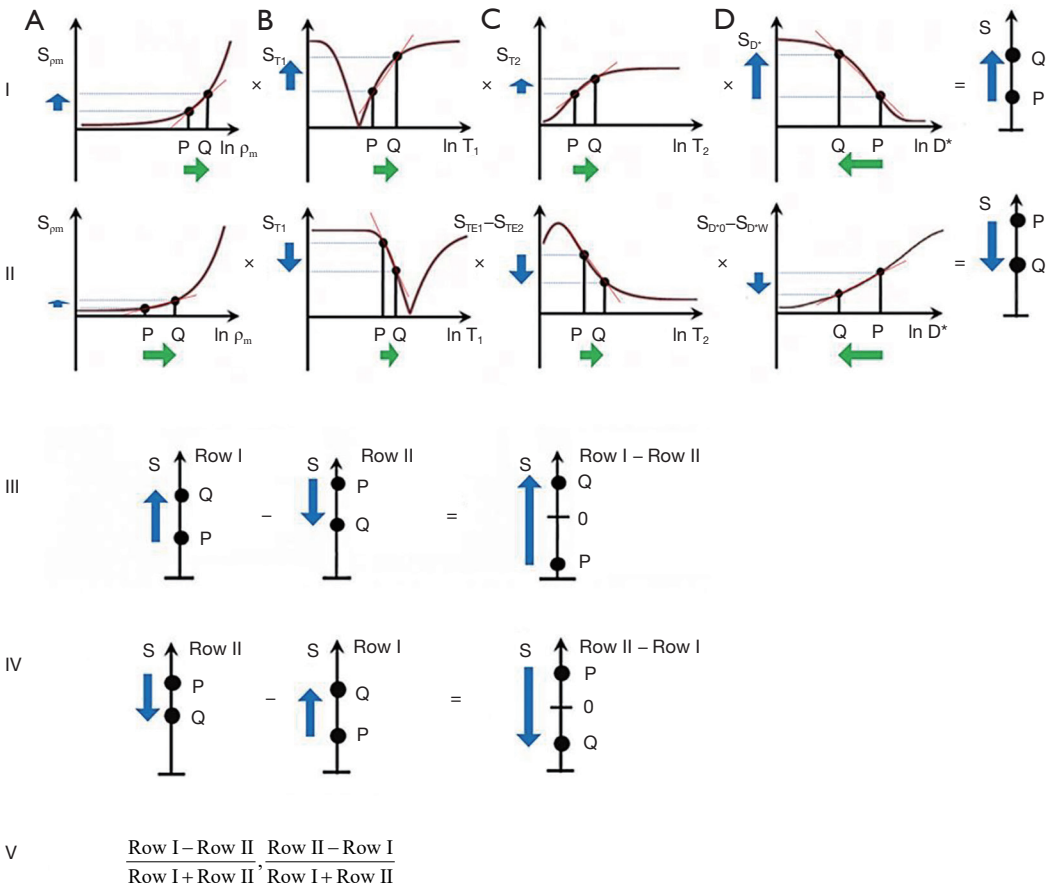

Figure 25 The SIREDS filters. The ρ_m, T_1 and T_2 and D* contrasts are synergistic and positive in Row I, and the T_1, T_2 and D* contrasts are synergistic and negative in Row II. In Row III, the subtraction (Row I minus Row II) results in overall synergistic positive contrast. Row IV shows the reverse subtraction. Row V shows the divided forms of the filters dSIREDS and drSIREDS which have increased T_1 contrast. SIREDS, subtracted IR echo diffusion subtraction; dSIREDS, divided SIREDS; drSIREDS, divided reverse SIREDS.

sequence was originally described with TIs chosen to null the signal from fluid and from white matter and these were combined by multiplication and normalized as the uni form of FLAWS (11). It was related to the MP2RAGE sequence which also multiplies and normalizes two IR sequences using the sum of the squares of the sequence signals in the denominator. The FLAWS sequence has been extended to include subtraction and division with the sum of the two sequences IR in the form of FLAWShc (FLAWS high contrast) and FLAWShco (FLAWS high contrast opposed) sequences which employ subtraction (12). It thus has common features with the dSIR and drSIR sequences. The FLAWdiv sequence is the shorter TI IR image divided by the longer TI IR image. This may become problematic when the signal from the longer TI IR image is nulled. Both FLAWShc and FLAWShco typically use wide mDs (ΔTI=156% at 1.5T [11] and ΔTI=130% at 7T [12]), not narrow mDs as with dSIR and drSIR sequences (e.g., ΔTIs=19–43% in this paper), and show lower contrast as a consequence. The FLAWShc sequence does not show high signal white-gray matter boundaries as the dSIR sequence does as a consequence of its wide mD. Unlike the FLAWShc and FLAWShco sequences, the dSIR and drSIR sequences are also combined synergistically with T_2 and D* sequence weightings.

FIR sequences

These obtain multiple IR images primarily for quantification of T_1 [e.g., MPnRAGE (13) and shMOLLI (Shortened MOdified Look-Locker Imaging) (14)]. The DESIRE

sequence can be used in this way but can also be used for selecting the best TI to null long T_2 components in tissue or tissues with different T_1s. The DESIRE sequence is included in both the subtraction and fitted categories.

scMRI

Synergistic contrast can arise in two main ways:

(i) A single TP can be used twice or more in a sequence. For example, T_1 can be used in the T_1 dependent TR segment of an IR sequence as well as the T_1 dependent TI segment. T_1 is also used twice in DIR sequences when two TI segments are multiplied together, and in the Subtracted IR (SIR) sequence when using the subtraction: short TI_s segment minus intermediate TI_i segment. The synergistic T_1 contrast from the SIR sequence can be increased further by using T_1 3–4 times in the form of dSIR and drSIR sequences.

Synergistic contrast may arise from repeated use of T_2 when imaging ultrashort T_2 tissues with an IR sequence using a long adiabatic inversion pulse to invert and null long T_2 signals while ultrashort T_2 tissues that are saturated by the inversion pulse recover, and following this after the 90° excitation pulse by ES. The two effects, firstly from the inversion pulse and nulling, and secondly from the decay in transverse magnetization produce synergistic negative contrast when there is an increase in T_2 in ultrashort T_2 tissues.

(ii) Two or more different TPs can also be used to produce synergistic contrast. Clinical pulse sequences have a basic structure consisting of ρm, T_1, and T_2 filters as seen in SE sequences. There are additional options which can be added such as those for T_1 dependent inversion pulses and D* sensitization. In many circumstances ρ_m is a minor determinant of contrast and T_1, T_2, and D* are major determinants. The most common change in TPs in disease is concurrent increases in ρ_m, T_1, T_2. In this situation with the SE sequence, the contrast developed by an increase in T_1 is negative while that developed by an increase in T_2 is positive, so that simultaneous increases in T_1 and T_2 produce opposed contrast and the net, or overall, contrast is reduced. To avoid this problem, T_1-weighted sequences use a short TE to minimize the opposed T_2 contrast, and T_2-weighted sequences use a long TR to minimize the opposed T_1 contrast. The dominant source of contrast in the resulting sequences is then a single TP, i.e., T_1 or T_2 and the sequences are described as T_1-weighted or T_2-weighted respectively. They are not synergistic for T_1 and T_2 contrast.

In particular circumstances, such as certain forms of the STIR and the DIR sequences, the T_1 contrast produced by an increase in T_1 is positive, and so is the T_2 contrast produced by an increase in T_2. The effects of the concurrent increases in T_1 and T_2 are therefore synergistic and typically result in high positive lesion contrast.

The contrast produced above from (i) a single TP, or (ii) two or more different TPs can be supplemented by increasing or decreasing signals from certain normal tissues and/or fluids. There may be little contrast between high signal lesions and high signal fat, long T_2 tissues, or fluids. Reduction in the normal signal from these latter tissues or fluids [using the same or different TPs as those used to create the original synergistic contrast in (i) and/or (ii)] can increase the contrast between the high signal lesions and the zero or low signal suppressed tissues and/or fluids. It may also result in a more appropriate dynamic range for the image.

In a tissue with a mixture of ultrashort T_2 and long T_2 tissues, for example, low abundance ultrashort T_2 tissues may only become apparent if the more abundant signals from the long T_2 tissues are reduced or suppressed. This also applies to edema in yellow bone marrow, where suppression of the more abundant fat signal may be necessary to show the lower concentration edema. Signals can also be increased for the same purpose.

The synergistic contrast produced in (i) and (ii) can also be supplemented by opposed contrast outside the region of interest.

One or both of mechanisms (i) and (ii) described above may be used in any one synergistic contrast sequence with, or without, supplementary synergistic contrast from suppression or increase of signals from normal tissues as well as the use of opposed contrast. Achievement of synergistic contrast requires a knowledge of the sign of sequence weighting of the TP-filters involved, as well as the sign of the change in each TP.

Image processing to achieve synergistic contrast

There are three situations within sequences where the ability to reverse the sign of the weighting of a filter of the sequence is important for achieving synergistic contrast.

Table 5 SIRES and rSIRES sequences image processing

#	ΔTP		Image processing	Disease examples
	T_1	T_2		
1	+	+	Row I (TI_s) nil (with les); (I minus II) then r ± d	Common diseases
			Row II (TIi) ES	
2	+	–	Row I (TI_s) ES; (I minus II) then r ± d	
			Row II (TI_i) nil (with les)	
3	–	+	Row I (TI_s) ES; (I minus II) then r ± d	
			Row II (TI_i) nil (with les)	
4	–	–	Row I (TI_s) nil (with les); (I minus II) then r ± d	
			Row II (TI_i) ES	Some hemorrhage, iron deposition, GBCA/MIOP accumulation

Changes in signs of ΔTP (ΔT_1 and ΔT_2) in disease, image processing to produce positive or negative T_1 and T_2 synergistic contrast, and disease examples. In #1 both T_1 and T_2 are increased, and Row I requires no processing except les. Row II uses ES. The subtraction (Row I minus Row II) produces a SIRES image. The reverse subtraction (r) produces a rSIRES image. Both can be divided to produce dSIRES and rSIRES images. The same principles apply to #2, 3 and 4. SIRES, subtracted IR echo subtraction; rSIRES, reverse SIRES; r, reverse; d, division; les, long echo subtraction; ES, echo subtraction; GBCA, gadolinium based contrast agent; MIOP, magnetic iron oxide particles; dSIRES, divided SIRES.

These are firstly, reversal of the sign of the T_1 contrast produced by a change in T_1 with IR sequences by using different TIs (together with m reconstruction). Secondly, reversal of the sign of T_2 contrast produced by a change in T_2 with SE T_2-filter by the subtraction: shorter TE filter minus longer TE filter i.e., ES. Thirdly, reversal of the sign of diffusion contrast produced by the PGSE D*-filter using the subtraction: low b value (e.g., 0–20 s/mm^2) filter minus high b value (e.g., 500–1,500 s/mm^2) filter i.e., DS. This ability to change the sign of the sequence TP-filter and the resulting contrast for T_1, T_2 and D* is crucial for creating synergistic contrast from either positive or negative changes in each of T_1, T_2 and D* in disease.

In addition to changing the sign of the sequence weighting of a filter within a sequence as above, it is also possible to reverse the order of subtraction of two sequences, and so reverse the contrast produced by the sequences. This is reverse (r) subtraction.

Using the same change in a TP twice or more in the same sequence may result in higher synergistic contrast than just using it once. Using changes in different TPs may also be effective in increasing overall contrast. This is because T_1, T_2 and D* often change concurrently in disease and using synergistic contrast to exploit the lesion contrast developed by each of these TPs may result in higher overall contrast. These are approaches targeted at increasing sequence sensitivity.

Image processing also includes late (very long TE) echo acquisition of signal from long T_2 fluids such as CSF. This can be helpful when CSF is at the top or bottom of the display dynamic range when white or gray matter would be preferred in this location. It is also of value in avoiding problems with partial volume effects simulating lesions.

It is also possible to specifically include image acquisitions for their use in image processing. This includes, for example, short TE sequences for subtraction from them of longer TE sequences.

Synergistic contrast can also be used to improve sequence specificity, for example, by using the reductions in both T_1 and T_2* produced by organic iron to provide high contrast visualization of its effects.

The main modification since the previous paper has been to include division in the image processing since it substantially increases T_1 synergistic contrast, usually as a final option after subtraction of filters and reversed subtraction of sequences (*Tables 5*,*6*).

Contrast at tissue boundaries

In the previous sections of this paper, contrast between two voxels has been considered, but there has been no reference to the space between voxels, or contrast at boundaries between two voxels.

In general terms, contrast detectability at boundaries

Table 6 SIREDS and rSIREDS sequences image processing

#	ΔTP			Image processing	Disease examples
	ΔT_1	ΔT_2	ΔD^*		
1	+	+	+	Row I (TI_s) DS (with les); (I minus II) then r ± d Row II (TI_i) ES (no D*)	Chronic disease, some tumors
2	+	+	−	Row I (TI_s) nil (with les); (I minus II) then r ± d Row II (TI_i) EDS	Acute disease (infarction, infection), many tumors
3	+	−	+	Row I (TI_s) EDS; (I minus II) then r ± d Row II (TI_i) nil (with les)	
4	+	−	−	Row I (TI_s) ES (no D*); (I minus II) then r ± d Row II (TI_i) DS (with les)	
5	−	+	+	Row I (TI_s) ES (no D*); (I minus II) then r ± d Row II (TI_i) DS (with les)	
6	−	+	−	Row I (TI_s) EDS; (I minus II) then r ± d Row II (TI_i) nil (with les)	
7	−	−	+	Row I (TI_s) EDS; (I minus II) then r ± d Row II (TI_i) nil (with les)	
8	−	−	−	Row I (TI_s) DS (with les) (I minus II) then r ± d Row II (TI_i) ES (no D*)	

Changes in ΔTP (ΔT_1, ΔT_2 and ΔD^*) in disease, image processing to produce positive or negative T_1, T_2 and D* synergistic contrast, and disease examples. In #1 Row I DS is used with les. In Row II ES is used. The subtraction Row I minus Row II is performed followed by the reverse subtraction ±division. The same type of pattern applies to #2–8. SIREDS, subtracted IR echo diffusion subtraction; rSIREDS, reverse SIREDS; r, reverse; d, division; les, long echo subtraction; ES, echo subtraction; DS, diffusion subtraction; EDS, combined echo and diffusion subtraction.

between two voxels can be related to $C_{ab}=\Delta S$ or $C_{fr}=\Delta S/S$ divided by the distance Δx between the voxels. Boundaries are more detectable when contrast is high and Δx is low, rather than in the opposite situation where contrast is low and Δx is high.

At a boundary between two pure tissues P and Q it is useful to define the tissue fraction f which is the proportion of the second tissue Q in a voxel containing a mixture of both tissues. The proportion of the other tissue P is then (1-f).

The T_1 of the mixture of the two tissues (P and Q) can be expressed as a function.

$$T_{1P,Q} = \Gamma\left(T_{1P}, T_{1Q}, f\right) \quad [17]$$

where $T_{1P,Q}$ is the T_1 of the mixture, T_{1P} is the T_1 of P, and T_{1Q} is the T_1 of Q. An example of this is shown in *Figure 26* (upper row, column B).

It is also useful to consider $\frac{\partial f}{\partial x}$ the change in tissue fraction with distance x. This is shown in *Figure 26* (upper row, column C) and may be gradual corresponding to a low value of $\frac{\partial f}{\partial x}(P)$ or more abrupt in parts corresponding to higher values of $\frac{\partial f}{\partial x}(Q)$.

Using the chain rule from differential calculus, for T_1

$$\frac{\Delta S}{S_{T1}\Delta x} \approx \frac{1}{S_{T1}} \cdot \frac{dS}{dx} = \frac{1}{S_{T1}} \cdot \frac{\partial S T_1}{\partial T_1} \cdot \frac{\partial T_1}{\partial f} \cdot \frac{\partial f}{\partial x} \quad [18]$$

where $\frac{\Delta S}{S_{T1}\Delta x}$ is the change in fractional contrast with distance x, S_{T1} is the T_1-filter signal, $\frac{dS}{dx}$ is a measure of detectable contrast, $\frac{\partial S_{T1}}{\partial T_1}$ is the first partial derivative of S_{T1} with respect to T_1 i.e., the sequence T_1-weighting, $\frac{\partial T_1}{\partial f}$ is

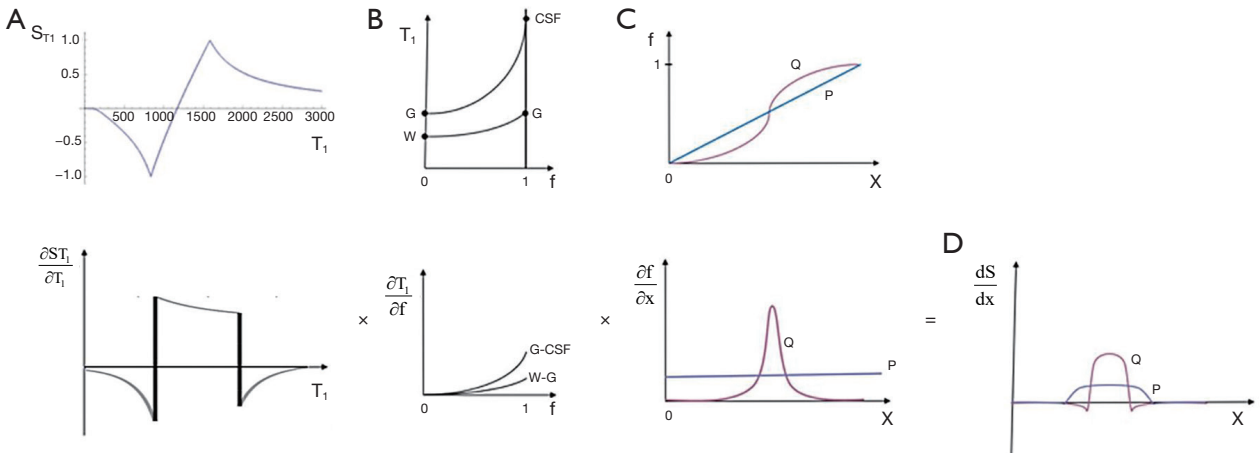

Figure 26 Fractional contrast between two tissues e.g., white and gray matter over distance x. In the upper row in column A is the T_1-filter of the sequence, in column B is the T_1 of the mixture of the two tissues plotted against tissue fraction f, and in column (C) is f plotted against distance x. In the lower row the partial derivatives of each of these functions are shown. The contrast with distance $\frac{dS}{dx}$ is the product of the three partial derivatives in columns (A), (B) and (C) and is shown in column (D) on the right.

Table 7 Partial derivatives $\frac{\partial S_{T1}}{\partial T_1}$, $\frac{\partial T_1}{\partial f}$ and $\frac{\partial f}{\partial x}$ which determine T_1-dependent change in signal or contrast with distance at boundaries

$\frac{\partial S_{T1}}{\partial T_1}$	$\frac{\partial T_1}{\partial f}$	$\frac{\partial f}{\partial x}$
Increasing T_1 sequence weighting from upper to lower (below)	Increasing value from upper to lower	Increasing value from upper to lower
SGE	White-gray matter	Gradual
IR	Gray matter-CSF	Abrupt
SIR	White matter-CSF	
dSIR		

SGE, spoiled gradient echo; IR, inversion recovery; SIR, subtracted IR; dSIR, divided SIR; CSF, cerebrospinal fluid.

the change in T_1 with tissue fraction f, and $\frac{\partial f}{\partial x}$ is the change in f with distance x. This is illustrated in *Figure 26* (lower row).

If the sequence weighting is high as within the mD of a dSIR sequence $\frac{\partial S_{T1}}{\partial T_1}$ is high (*Table 7*). In the brain $\frac{\partial T_1}{\partial f}$ is increased from white-gray matter to gray matter-CSF to white matter-CSF at boundaries between tissue fluids. $\frac{\partial f}{\partial x}$ increases as the transition from one tissue changes from gradual to abrupt.

If one or more of the partial derivatives in Eq. [18] is zero, the tissue appears flat on the image. This can occur with "dark bone" imaging where the SGE sequence has a low flip angle and short TE, and is insensitive to T_1 changes so that $\frac{\partial S_{T1}}{\partial T_1} = 0$ (but not to low ρ_m which accounts for the bone contrast). If the T_1s of P and Q are the same $\frac{\partial T_1}{\partial f} = 0$, then no contrast results. If $\frac{\partial f}{\partial x} = 0$, i.e., there is no change in the proportions of the two tissues, no contrast results.

At a boundary between two tissues the actual T_1 of the voxels with mixtures of tissues within them spans the range of T_1 values between the two tissues. This is shown in *Figure 27*. If the T_1-filter is such that a T_1 value between those of the two tissues results in a high value of S, a high signal line results at the boundary between the two tissues, as seen in *Figure 28*. The width and location of the line is dependent on the slope of the filter and the gradient of T_1

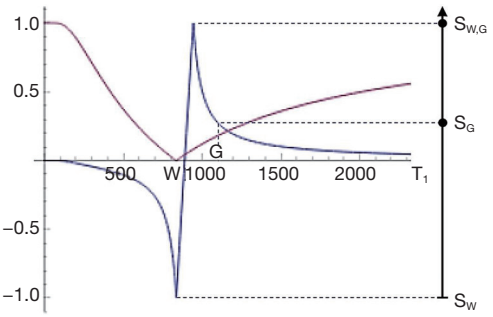

Figure 27 A dSIR filter with a narrow mD extending from white matter (W) to a $T_{1W,G}$ between white matter and gray matter (G) (blue) and a white matter nulled T_1-filter e.g., from MP-RAGE (pink). The peak signal ($S_{W,G}$) appears between W and G in the X axis where there are partial volume effects producing the $T_{1W,G}$ between W and G matter corresponding to the peak signal $S_{W,G}$. This results in a high signal line between white and gray matter as shown in *Figure 28*. dSIR, divided subtracted inversion recovery; MP-RAGE, magnetization prepared rapid acquisition gradient echo.

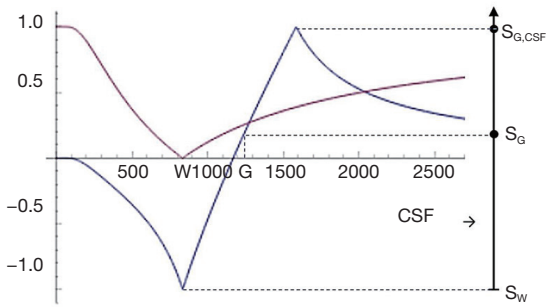

Figure 29 dSIR filter (blue filter) with the first TI nulling white matter (W) and a wide mD with the second TI nulling at a $T_{1G,CSF}$ greater than the T_1 of gray matter (G) corresponding to a mixture of gray matter and CSF. The pink filter is that from a white matter nulled IR sequence e.g., MP-RAGE. The signal $S_{G,CSF}$ is greater than that of the signal from gray matter S_G and that from white matter S_W, and corresponds to the line between gray matter and CSF seen outside of the brain in *Figure 30*. dSIR, divided subtracted inversion recovery; CSF, cerebrospinal fluid; MP-RAGE, magnetization prepared rapid acquisition gradient echo.

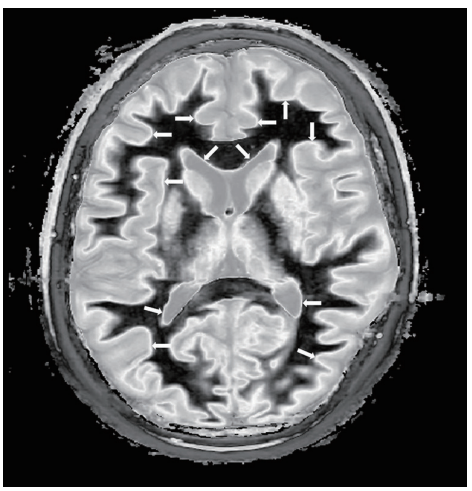

Figure 28 dSIR image with the first TI nulling white matter (W) and the second TI less than that needed to null gray (G) matter. High signal boundaries are seen between W and G matter as well as between white matter and CSF (arrows). dSIR, divided subtracted inversion recovery; CSF, cerebrospinal fluid.

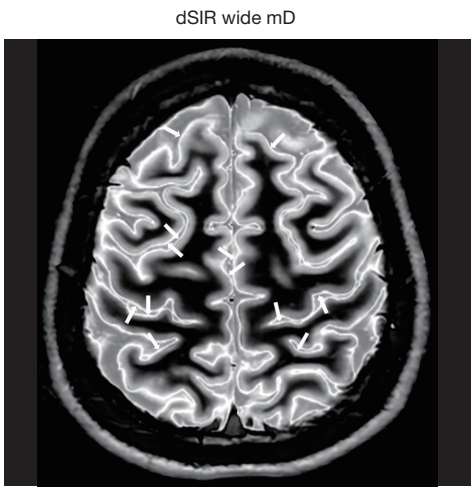

Figure 30 dSIR image of the brain using a wide mD with the second TI longer than that needed to null cortical gray matter (TI_s=350 ms and TI_i=800 ms, ΔTI=130% at 3T). High signal boundaries are seen outside of the brain between the cortex and CSF (arrows). dSIR, divided subtracted inversion recovery; CSF, cerebrospinal fluid.

with f as well as the gradient of f with x as shown in *Figure 26* (lower row). The high signal boundary at the white-gray matter boundary inside the brain in *Figure 28* was obtained using a narrow mD.

Figure 29 shows use of a wide mD filter in which maximum signal is reached with a T_1 between those of gray matter and CSF. This arises from partial volume effects between gray matter and CSF, and produces a high signal boundary between gray matter and CSF outside of the brain as shown in *Figure 30*.

Boundaries can also be seen around lesions that increase their T_1s beyond the T_1 of the upper limit of the mD. The lesion then shows a high signal margin and a lower signal center because the T_1 of the lesion is higher than the T_1 resulting in maximum signal at the boundary.

The width and location of the boundary e.g., white-gray matter or gray matter-CSF can be changed by choice of mD and the width of the boundary can be changed, altering the slope and location of the maximum signal of the T_1-filter. In general, wider mDs result in greater width of tissue boundaries.

The conventional wisdom on partial volume effects between tissues in the brain with SE dcs is that the signal of voxels containing two tissues such as white and gray matter is intermediate between those of the two constituent tissues. The appearances in *Figures 28*,*30* are therefore counter-intuitive and difficult to explain without reference to TP-filters and the CCT.

High signal boundaries provide a useful basis for locating lesions as well as for segmentation of tissues and following changes in space in serial imaging studies as described in the next section.

Small change regimes

In general terms, there is often no particular premium in clinical MRI in demonstrating large changes with even greater contrast, so the emphasis with MASDIR sequences is on demonstrating lesions where there are only small changes in TPs with sufficient contrast for the images to be of diagnostic value. The emphasis has therefore been on imaging regimes to detect small changes and ideally monitor them over time to follow their natural history, and/or the effects of treatment.

Increased sensitization in the mD is accompanied by a decreased width of the mD. This combination is particularly appropriate for detecting small changes in T_1 in specific tissues where high contrast can be produced by a small change in T_1. Small changes from normal are commonly seen in earlier and more subtle forms of disease.

On MR images changes may be in signal or contrast, and in space, e.g., increase or decrease in size of normal structures, or in both signal/contrast and space.

Differences/changes in signal may be anatomical on single images, but may also include changes in space with growth and atrophy for example.

Perturbations in signal due to change in T_1 occur with pre and post gadolinium-based contrast agent (GBCA) administration, inhalation of 100% O_2, perfusion and angiography, as well as with fMRI.

Disease usually involves both changes in signal and space, but in some cases the changes in space are small and the situation can be treated as a change in signal.

The changes in signal and space from normal in a single image may change over time in serial studies as part of the natural history of the disease and/or the result of therapy. In the situation where changes are small, rigid body registration is well suited to accurately aligning images obtained on two or more occasions so that genuine changes can be distinguished from artefactual differences due to variation in slice alignment.

This has been performed with isotropic 3D SGE sequences and a system of interpretating images including distinguishing pure signal changes from spatial changes where possible has been described (15). 3D isotropic MASDIR sequences using MP-RAGE/BRAVO (BRAain VOlume) type data acquisitions with SIR/rSIR and or dSIR/drSIR image processing offer increased sensitivity to changes in contrast. They also offer high contrast, high resolution definition of boundaries to improve detection of changes in space. It is likely that this will be a significant application of MASDIR sequences.

Examples

Application of these principles can be seen in a case of multiple sclerosis (MS) (*Figure 31*). In the upper row the T_2-FLAIR images demonstrate focal lesions in the pons and deep white matter of the left hemisphere. Normal white matter on the image is seen in the cerebellum and appears dark. The dSIR image shows very extensive change in white matter in the pons and adjacent cerebellum as high signal areas (arrows). These abnormalities are not seen on the T_2-FLAIR image. *Figure 32* is an enlarged version of the dSIR image in the upper row and *Figure 33* is an enlarged version of the dSIR image in the lower row.

In the lower row of *Figure 31* the T_2-FLAIR image shows two focal lesions (arrows). These are seen on the dSIR image (*Figure 31*, lower row, right) and on the expanded image in *Figure 33*. There is extensive involvement of white matter which appears as higher signal regions compared with the normal white matter regions which are dark. High signal lines are seen at the boundaries between white matter and gray matter as well as between white matter and CSF. The lesion in the posterior deep white matter on the left (long white arrow) shows the "iceberg sign". The

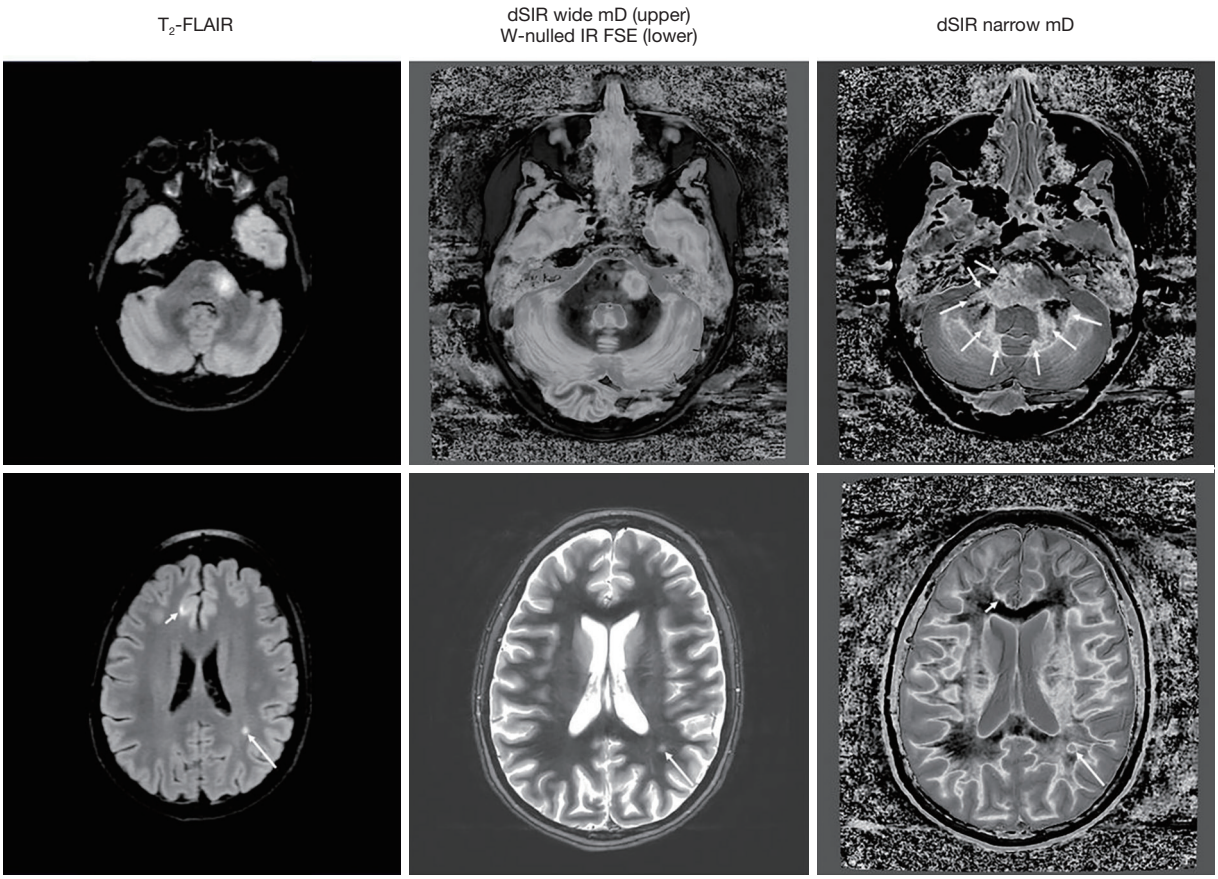

Figure 31 Case of multiple sclerosis. T_2-FLAIR (left column), dSIR wide mD (upper row) and white matter nulled W-nulled IR FSE (lower row) (center column) and narrow mD dSIR (right column) images [TI_s=350 ms and TI_i=800 ms (wide mD, ΔTI=130%) as well as TI_s=350 ms and TI_i=500 ms (narrow mD, ΔTI=43%) at 3T]. In the upper row, a lesion is seen on the T_2-FLAIR sequence in the left pons. This lesion is seen with higher contrast on the wide mD dSIR image (upper row, center column). In the upper row right column, the narrow mD dSIR image shows extensive involvement of the pons and much of the cerebellum beyond the lesion. These areas have high signals (arrows). The only normal areas are in the cerebellum and appear dark. dSIR, divided subtracted inversion recovery. In the lower row, lesions are seen on the T_2-FLAIR sequence (left column) and the W-nulled IR FSE (center column) (arrows). On the narrow mD dSIR image (lower row, right column) there is extensive involvement of the white matter which is shown as higher signal areas. Normal white matter is black and the abnormal areas are gray or white. Well-defined boundaries are seen between white matter and gray matter as well as between white matter and CSF around the lateral ventricles. The lesion in the left deep white matter on the T_2-FLAIR image (arrow) is shown with a circular rim on the narrow mD dSIR image (arrow). The subcortical lesion on the T_2-FLAIR image (arrow) is seen as high signal on the narrow mD dSIR image (arrow). T_2-FLAIR, T_2-weighted-fluid-attenuated inversion recovery; dSIR, divided subtracted inversion recovery.

abnormal area is surrounded by a high signal line (longer white arrow). Beyond the lesion, there are extensive areas of abnormal white matter which have signals greater than the normal level of black. These abnormal areas are not seen with the T_2-FLAIR sequence.

In the same case T_2-wSE images are compared with dSIR images (*Figure 34*). No definite abnormality is seen on the T_2-wSE image (*Figure 34A*) but three focal lesions are seen on the dSIR images (long arrows). The corticospinal tracts are also abnormal (short arrows) and there are areas of increased signal in the white matter (normal white matter appears black).

At a higher level (*Figure 35*), an obvious focal lesion is only seen with dSIR (long arrow). Abnormalities are seen in the corticospinal tracts (short arrows) and elsewhere in the white matter.

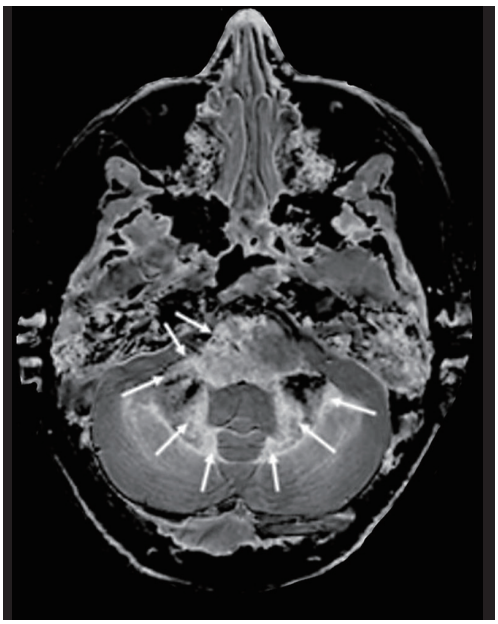

Figure 32 Enlarged version of the narrow mD dSIR image shown in the upper row, right column in *Figure 31*. Abnormal areas in the pons and cerebellum are highlighted (white arrows). Normal white matter in the cerebellum is dark. The boundary between normal and abnormal white matter in the cerebellum, and gray matter in the cerebellum is seen as a high signal line posteriorly. There is extensive abnormality in this image outside of the left pontine lesion in areas that appear normal on the corresponding T_2-FLAIR sequence in *Figure 21*. dSIR, divided subtracted inversion recovery; T_2-FLAIR, T_2-weighted-fluid-attenuated inversion recovery.

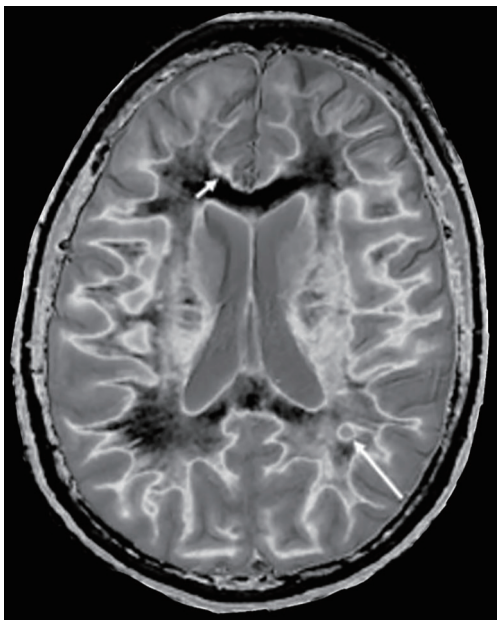

Figure 33 Enlarged version of the narrow mD dSIR image shown in the lower row, right column in *Figure 31*. The two lesions seen on the T_2-FLAIR sequence are shown (short and long white arrows). Normal white matter is dark. The lower lesion (longer white arrow) has a high signal margin and a lower signal center. Abnormal areas are seen in the deep white matter. These show increased signal from normal black up to a maximum equal to the signal level at the boundaries between white and gray matter. These boundaries show high contrast as do the boundaries between white matter and CSF around the lateral ventricles. There is much more abnormality in the central white matter shown on the dSIR sequence than on the corresponding T_2-FLAIR image in *Figure 31*. The lower lesion shows the "iceberg sign" where the abnormal area seen on the T_2-FLAIR sequence is surrounded by a white line on the dSIR image and there is extensive additional abnormality in white matter surrounding the lesion. dSIR, divided subtracted inversion recovery; T_2-FLAIR, T_2-weighted-fluid-attenuated inversion recovery.

Practical issues

(i) A common cause of failure to show contrast with the SIR group of sequences is using an initial TI (e.g., to null white matter) which is too long. The nulling TI needs to be precisely targeting often at the transition between normal and abnormal T_1 values.

(ii) Another cause of failure to show high contrast with SIR type sequences is a ΔTI which is too wide. This provides broad coverage, but not high amplification for small changes in T_1. ΔTI needs to be matched to the expected changes in T1.

(iii) Low contrast may arise in a lesion if the T_1 of the lesion is markedly increased, so that it "overshoots" the longer TI. It may then show mid-range signal (usually with a high signal boundary around it).

(iv) High contrast may not be seen if the chosen mD does not allow for a significant increase/decrease in T_1.

(v) There are a wide range of factors which affect the nulling TI. Fifteen of these are listed in *Table 8* and one or more of them may account for a failure to null signal when expected.

(vi) Another problem may be that contrast is already high, and trying to show a further increase with SIR type sequences or the addition of T_2 with SIRES type sequences may be difficult.

(vii) There are advantages in specifically matching the initial nulling T_1 and change in T_1 with disease to ΔTI for sign and size of change as far as possible to

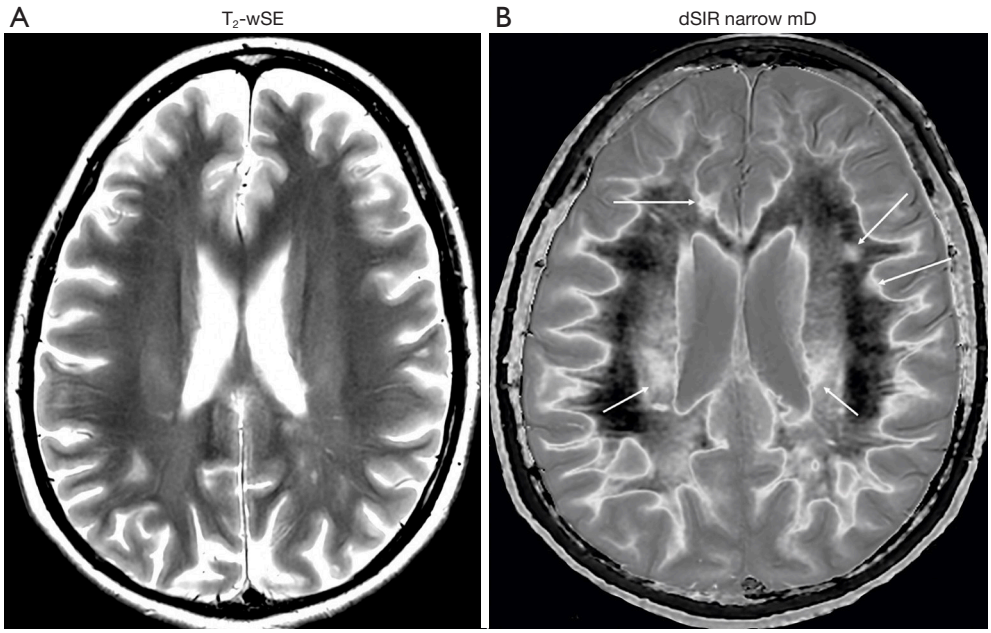

Figure 34 Case of multiple sclerosis. Comparison of T_2-wSE (A) and narrow mD dSIR (B) images. No abnormality is seen on the T_2-wSE image but three focal lesions are seen on the dSIR image (long arrows). The corticospinal tracts are also abnormal (short arrows), and many other areas of white matter are abnormal and show higher signal than normal white matter which is black. A high signal boundary is seen between white matter and cortical gray matter as well as between white matter and CSF at the boundary around the lateral ventricles. dSIR, divided subtracted inversion recovery; CSF, cerebrospinal fluid.

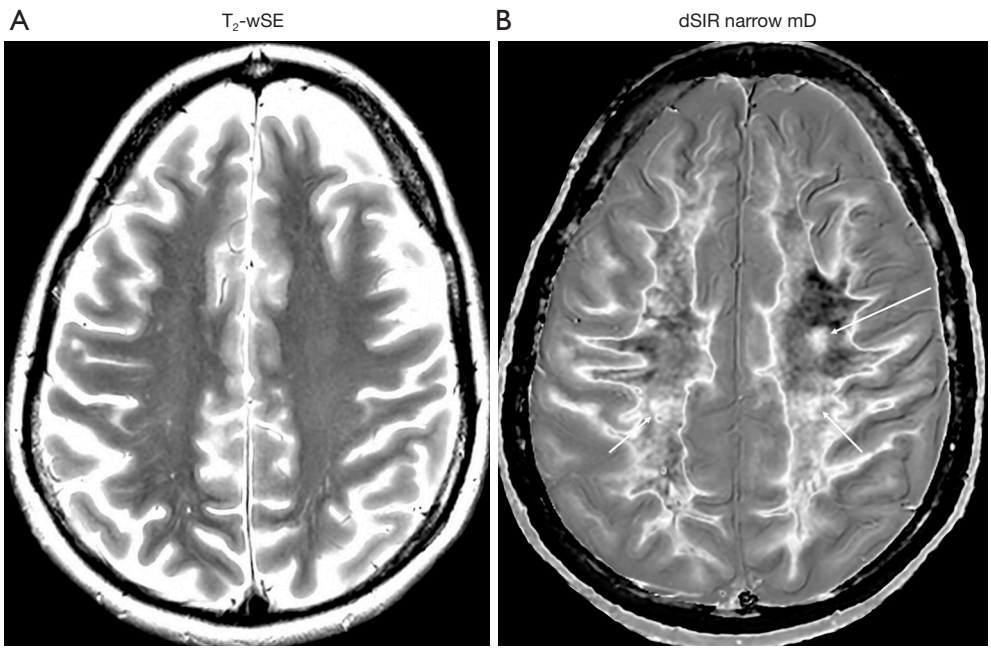

Figure 35 Case of multiple sclerosis. Comparison of T_2-wSE (A) and narrow mD dSIR (B) images at a higher level. A focal lesion not seen on the T_2-wSE is seen on the dSIR image (long arrow) and other abnormalities are seen in the corticospinal tracts (short arrows) as well as elsewhere in the white matter. High signal boundaries are seen between white matter and cortical gray matter. These features are not seen on the T_2-wSE image (A). dSIR, divided subtracted inversion recovery.

Table 8 Causes of changes in the TI for nulling tissues

Imaging techniques	Changes in T_1
Field strength B_0	Change in T_1 with age
Different TRs	Change in T_1 with site in organ
Different recovery times (with different TIs)	Change in T_1 with disease
Efficiency of B_1 pulse	Change in T_1 with contrast agents
Inhomogeneity of B_1	Change in T_1 with 100% O_2 inhalation
Data collection e.g., gradient echo *vs.* SE	Change in T_1 with temperature
Fast recovery	Change in T_1 with formalin fixation
Fat saturation	Uninverted ultrashort T_2 species
	Decrease in observed/effective T_1 due to magnetization transfer

SE, spin echo.

take advantage of the near linear relationship between dSIR and drSIR signals and T_1 as described in the Appendix 1.

(viii) Not using les with SIRES and rSIRES means that CSF signal may be at the top or bottom of the display gray scale range. This may produce partial volume effects and make lesions less obvious.

(ix) For SIR sequences the prostate is in many ways a mirror reflection of the brain. In disease, T_1 and T_2 are reduced. It is therefore useful to start with the longest T_1 tissue PZ and use rSIR filters and work towards the shorter T_1 TZ, and beyond this the shorter T_1 of capsular tissue to establish nulling values of TI for the PZ and TZ.

(x) The location of boundaries with SIR and dSIR sequences i.e., whether they are internal or external to the cortex of the brain provides a reliable indication of whether the second TI is too short or too long.

(xi) Partial volume effects at high signal boundaries may simulate lesions.

(xii) Misregistration of images may produce high and low signal boundaries.

Discussion

The paper summarizes advances in TP-filters and the CCT, MASDIR sequences, and scMRI and uses concepts from each of these to develop a formalism for understanding contrast at tissue boundaries, small change regimes and a method for T_1 quantitation. In images of MS, the archetypal disease for neuroinflammation, this combination outclasses the gold standard sequences T_2-FLAIR and T_2-wSE. The approaches are likely to have significant applications in brain, body and musculoskeletal systems.

The work has a mathematical basis using differential calculus to understand TP-filters and the CCT, as well as contrast at boundaries. The basic operations of arithmetic, namely multiplication, addition, subtraction and division are used to combine IR sequences. The graphics used to understand contrast is accessible using a basic level mathematical App such as WolframAlpha.

In the development of MRI many aspects such as image acquisition, reconstruction, processing and quantitation have primarily been the domain of physicists and other scientists. However, image contrast and clinical application of it has usually been the domain of radiologists and other clinicians. This latter activity involving sequence preparations, basic acquisitions and image processing has been an area where radiologists and clinicians can make a specific contribution to clinical MRI.

The illustrated examples highlight the brain since historically this is where clinical MRI began with concepts developed for the brain subsequently applied to the body, musculoskeletal system and cardiovascular system as well as to children. Normal white and gray matter provide an obvious point of reference for assessing contrast between two tissues, and the concepts for differentiating them can be applied to differentiating two other tissues i.e., normal and abnormal.

Prostate tumors in the peripheral and transitional zones are an interesting example where the T_1 and T_2 of tumors is decreased rather than increased (which is the common

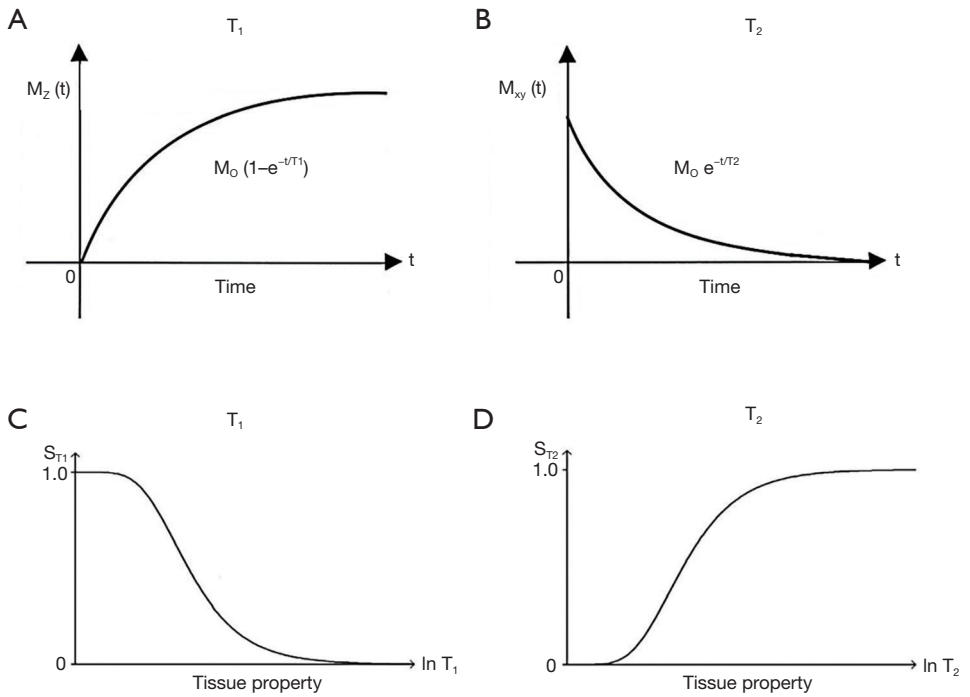

Figure 36 The upper row shows exponential T_1 dependent recovery of longitudinal magnetization M_Z (left) and T_2 dependent decay of transverse magnetization M_{XY} (right) with the X axes time t. The lower row shows a T_1-filter (left) and a T_2-filter (right). The X axes of these filters are the natural logarithms of the tissue properties T_1 and T_2 respectively. The slopes of the curves describing T_1 and T_2 dependent behavior of the signals in the upper row are reversed in the lower row when T_1 and T_2-filters are used to describe T_1 and T_2 dependent behavior of the signals (left and right columns).

pattern elsewhere in the nervous system and body). This approach is in many ways a mirror reflection of what has been done in the brain. The baseline tissue is the long T_1 PZ followed by the shorter T_1 PZ (*Figure 2*). Reductions in T_1 are seen in tumors so rSIR and rdSIR are used primarily rather than SIR and dSIR as in the brain.

There are a number of aspects to this work which appear counter-intuitive:

(i) In the Bloch equations for the SE sequence, the TP-filters approach assigns the variable time two constant values TR and TE, and treats the two time constants T_1 and T_2 as variables. The resulting filters which describe T_1 and T_2 effects on MRI images have the opposite slopes to those shown for T_1 and T_2 in graphical representations of the Bloch equations (*Figure 36*). Thus, instead of T_1 describing an increasing exponential, the T_1-filter describes a decreasing function (A and C, in the T_1 column). Instead of T_2 describing a decreasing exponential decay, the T_2-filter takes the form of an increasing sigmoid function (B and D, in the T_2 column). This can be a source of confusion.

(ii) The application of commonly used MASDIR sequences also appears counter-intuitive. In the brain, to visualize white matter, the first step with the SIR sequence is to use a TI to null it. The next step is to null other tissues (e.g., abnormal tissues) with T1s close to that of white matter. Following this, the remaining signal is subtracted one way, and then the other way. What signal is left can be divided and further subtractions and reversals may follow for T_2 and D*. After these operations, it seems unlikely that any useful signal will be left, or at best it will have a low SNR and not be of diagnostic use. The impetus to acquire nulled IR sequences and image process them in the way described came from mathematical modelling, not empirical observations of images.

(iii) The sequence can also be counter-intuitive as far as tissue boundaries are concerned. The accepted view for partial volume effects at boundaries between white and gray matter, as well as between

gray matter and CSF, is that their signal intensity is intermediate between those of the tissues or fluids involved. However, SIR and dSIR images often show boundaries between tissues with signals much higher than those of either of the constituent tissues or fluids.

(iv) It also seems improbable that it is possible to achieve 5–15 times the contrast of already high contrast conventional intermediate TI IR sequences such as MP-RAGE and IR FSE.

(v) It is also possible to obtain T_1 values directly from acquired dSIR and drSIR images without having to create T_1 maps. The maps have the same high contrast and high spatial resolution as the original images.

(vi) The signal intensities of CSF are often intermediate rather than high as in T_2-wSE sequences, or low as in T_1-weighted SGE or SE and T_2-FLAIR sequences and this can undermine belief in the integrity of the imaging process.

(vii) Very highly T_1-weighted SIR and dSIR sequences look "T_2-weighted" in that gray matter has a higher signal than white matter as is the case with T_2-wSE sequences.

Resolution of these issues often follows from use of TP-filter graphics rather than the use of conventional qualitative weighting. As a result, understanding of contrast produced by MASDIR sequences can be easier for newcomers to the field than for experienced practitioners who may have to become accustomed to quite new appearances of images and unlearn traditional explanations for MR appearances that have taken them years to acquire.

Acknowledgments

The authors thank Dr. Nivedita Agarwal for providing Figure S1.

Funding: This work was supported by National Institutes of Health (Nos. R01AR062581, R01AR068987, R01AR079484 and R21AR075851), the VA Clinical Science Research & Development Service (No. I01CX002211), and GE Healthcare (Nos A-31, A-32 and A-33) as well as from Kānoa-RDU, New Zealand and Trust Tairāwhiti, New Zealand.

Footnote

Conflicts of Interest: All authors have completed the ICMJE uniform disclosure form (available at https://qims.amegroups.com/article/view/10.21037/qims-22-394/coif). JD serves as an unpaid editorial board member of *Quantitative Imaging in Medicine and Surgery*. GMB is a consultant to Magnetica. The other authors have no conflicts of interest to declare.

Ethical Statement: The authors are accountable for all aspects of the work in ensuring that questions related to the accuracy or integrity of any part of the work are appropriately investigated and resolved.

References

1. Young IR, Szeverenyi NM, Du J, Bydder GM. Pulse sequences as tissue property filters (TP-filters): a way of understanding the signal, contrast and weighting of magnetic resonance images. Quant Imaging Med Surg 2020;10:1080-120.
2. Ma YJ, Fan S, Shao H, Du J, Szeverenyi NM, Young IR, Bydder GM. Use of Multiplied, Added, Subtracted and/or FiTted Inversion Recovery (MASTIR) pulse sequences. Quant Imaging Med Surg 2020;10:1334-69.
3. Ma YJ, Shao H, Fan S, Lu X, Du J, Young IR, Bydder GM. New options for increasing the sensitivity, specificity and scope of synergistic contrast magnetic resonance imaging (scMRI) using Multiplied, Added, Subtracted and/or FiTted (MASTIR) pulse sequences. Quant Imaging Med Surg 2020;10:2030-65.
4. Yu AC, Badve C, Ponsky LE, Pahwa S, Dastmalchian S, Rogers M, Jiang Y, Margevicius S, Schluchter M, Tabayoyong W, Abouassaly R, McGivney D, Griswold MA, Gulani V. Development of a Combined MR Fingerprinting and Diffusion Examination for Prostate Cancer. Radiology 2017;283:729-38.
5. Panda A, Obmann VC, Lo WC, Margevicius S, Jiang Y, Schluchter M, Patel IJ, Nakamoto D, Badve C, Griswold MA, Jaeger I, Ponsky LE, Gulani V. MR Fingerprinting

and ADC Mapping for Characterization of Lesions in the Transition Zone of the Prostate Gland. Radiology 2019;292:685-94.
6. Bydder GM, Young IR. MR imaging: clinical use of the inversion recovery sequence. J Comput Assist Tomogr 1985;9:659-75.
7. Redpath TW, Smith FW. Technical note: use of a double inversion recovery pulse sequence to image selectively grey or white brain matter. Br J Radiol 1994;67:1258-63.
8. Marques JP, Kober T, Krueger G, van der Zwaag W, Van de Moortele PF, Gruetter R. MP2RAGE, a self bias-field corrected sequence for improved segmentation and T1-mapping at high field. Neuroimage 2010;49:1271-81.
9. Ma YJ, Searleman AC, Jang H, Wong J, Chang EY, Corey-Bloom J, Bydder GM, Du J. Whole-Brain Myelin Imaging Using 3D Double-Echo Sliding Inversion Recovery Ultrashort Echo Time (DESIRE UTE) MRI. Radiology 2020;294:362-74.
10. Ma YJ, Jang H, Wei Z, Cai Z, Xue Y, Lee RR, Chang EY, Bydder GM, Corey-Bloom J, Du J. Myelin Imaging in Human Brain Using a Short Repetition Time Adiabatic Inversion Recovery Prepared Ultrashort Echo Time (STAIR-UTE) MRI Sequence in Multiple Sclerosis. Radiology 2020;297:392-404.
11. Beaumont J, Saint-Jalmes H, Acosta O, Kober T, Tanner M, Ferré JC, Salvado O, Fripp J, Gambarota G. Multi T1-weighted contrast MRI with fluid and white matter suppression at 1.5 T. Magn Reson Imaging 2019;63:217-25.
12. Beaumont J, Gambarota G, Saint-Jalmes H, Acosta O, Ferré JC, Raniga P, Fripp J. High-resolution multi-T1 -weighted contrast and T1 mapping with low B 1 >+ sensitivity using the fluid and white matter suppression (FLAWS) sequence at 7T. Magn Reson Med 2021;85:1364-78.
13. Kecskemeti S, Samsonov A, Hurley SA, Dean DC, Field A, Alexander AL. MPnRAGE: A technique to simultaneously acquire hundreds of differently contrasted MPRAGE images with applications to quantitative T1 mapping. Magn Reson Med 2016;75:1040-53.
14. Mozes FE, Tunnicliffe EM, Moolla A, Marjot T, Levick CK, Pavlides M, Robson MD. Mapping tissue water T1 in the liver using the MOLLI T1 method in the presence of fat, iron and B0 inhomogeneity. NMR Biomed 2019;32:e4030.
15. Bydder GM. The Mackenzie Davidson Memorial Lecture: detection of small changes to the brain with serial magnetic resonance imaging. Br J Radiol 1995;68:1271-95.

Cite this article as: Ma YJ, Moazamian D, Cornfeld DM, Condron P, Holdsworth SJ, Bydder M, Du J, Bydder GM. Improving the understanding and performance of clinical MRI using tissue property filters and the central contrast theorem, MASDIR pulse sequences and synergistic contrast MRI. Quant Imaging Med Surg 2022;12(9):4658-4690. doi: 10.21037/qims-22-394

Appendix 1 Features of the dSIR and drSIR filters including use of them for T_1 mapping

The signals S_s and S_i for two long TR IR T_1-filters with short and intermediate TIs, TI_s and TI_i respectively are given by:

$$S_S = 1 - 2e\left(-TI_S/T_1\right) \quad [19]$$

and

$$S_i = 1 - 2e\left(-TI_i/T_1\right) \quad [20]$$

Performing the subtraction: magnitude of the IR signal $|S_s|$ in Eq. [19] minus magnitude of the IR signal $|S_i|$ in Eq. [20] gives the signal of the SIR filter S_{SIR} which is equal to $-S_s - S_i$ i.e.:

$$S_{SIR} = 2e\left(-TI_S/T_1\right) + 2e\left(-TI_i/T_1\right) - 2 \quad [21]$$

Addition of the magnitudes of the two IR signals $|S_s|$ and $|S_i|$ in Eqs. [19,20] S_{AIR} is equal to $-S_s + S_i$ i.e.:

$$S_{AIR} = 2e\left(-TI_S/T_1\right) - 2e\left(-TI_i/T_1\right) \quad [22]$$

Division of the signal of the subtraction filter S_{SIR} in Eq. [21] by the signal of the addition filter S_{AIR} in Eq. [22] gives the signal of the S_{dSIR} filter:

$$S_{dSIR} = \frac{e\left(-TI_S/T_1\right) + e\left(-TI_i/T_1\right) - 1}{e\left(-TI_S/T_1\right) - e\left(-TI_i/T_1\right)} \quad [23]$$

While this expression is accurate, it does not provide easy insight into the properties of the S_{dSIR} filter. To do this a linear regression of the form y = mx + c between the end-points of the mD produced by fitting a straight line between the first and last points of the mD (ie first point x = TI_s / ln 2 and y = 1, and last point x = TI_i / ln 2 and y = –1) can be used as an approximation for the S_{dSIR} filter so:

$$S_{dSIR} \approx \frac{\ln 4}{\Delta TI} T_1 - \frac{\Sigma TI}{\Delta TI} \quad [24]$$

Where $\Delta TI = TI_s - TI_i$ and $\Sigma TI = TI_s + TI_i$

The same applies to the drSIR filter except that it has a negative slope and a positive offset. Its signal equation is:

$$S_{drSIR} \approx -\frac{\ln 4}{\Delta TI} T_1 + \frac{\Sigma TI}{\Delta TI} \quad [25]$$

The expressions in Eq. [24,25] capture four key features of the dSIR filter, firstly, they show linear change of signal with T_1 in the mD, secondly, they have slopes equal to ln 4/ΔTI and -ln 4/ΔTI respectively, thirdly they show high sensitivity to small changes in T_1 when ΔTI is small, and fourthly the equations can be used to map T_1 since for S_{dSIR} and S_{drSIR}:

$$T_1 \approx \frac{\Delta TI}{\ln 4} S_{dSIR} - \frac{\Sigma TI}{\ln 4} \quad [26]$$

$$T_1 \approx -\frac{\Delta TI}{\ln 4} S_{drSIR} + \frac{\Sigma TI}{\ln 4} \quad [27]$$

The S_{dSIR} and S_{drSIR} maps show high contrast and high spatial resolution as for the two source images since they are linear voxel rescalings of these images (e.g., *Figure 37*) with the two caveats (i) it only applies to T_1s in the mD, and (ii) the reasoning applies to long TR IR images. If the TR is not long enough, correction of the T1 values is likely to be needed.

For absolute contrast, Cab from Eqs. [24,25] and using a linear X axis:

https://dx.doi.org/10.21037/qims-22-394

$$C_{ab} = \Delta S_{dSIR} \approx \frac{\ln 4}{\Delta TI} \Delta T_1 \quad [28]$$

and

$$C_{ab} = \Delta S_{drSIR} \approx -\frac{\ln 4}{\Delta TI} \Delta T_1 \quad [29]$$

Thus the absolute contrast for the dSIR and drSIR filters is proportional to the reciprocal of ΔTI as well as the difference/change in T_1.

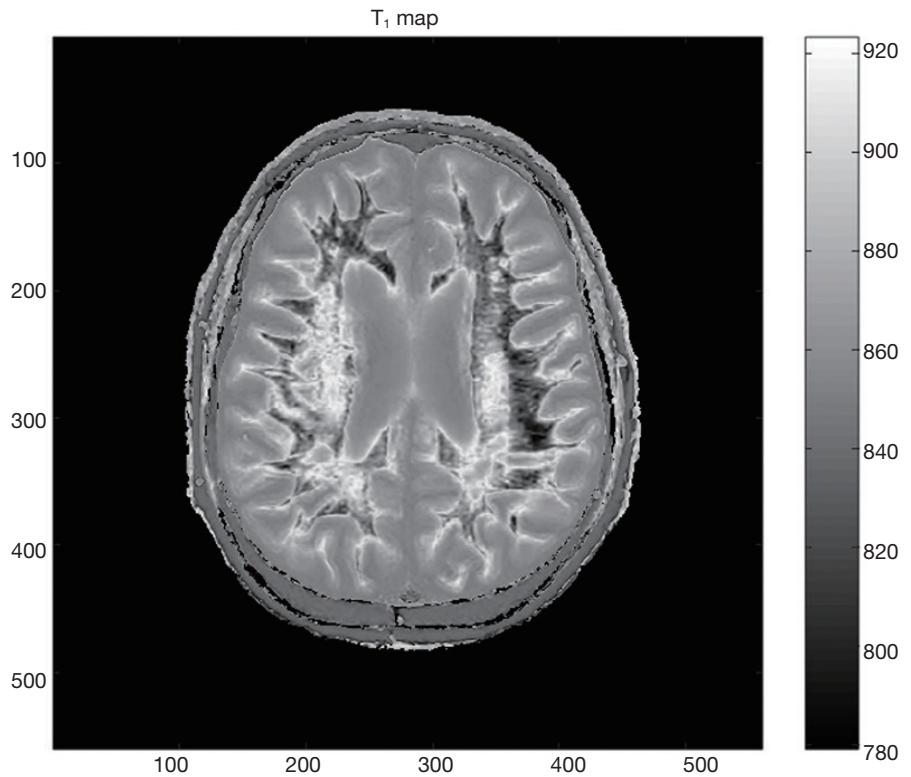

Figure S1 Rescaled dSIR image and T_1 map in a patient with small vessel disease showing T_1 values within the mD which is in white matter (TI_s=540 ms, TI_l=640 ms, ΔTI=19%, TR=6,000 ms at 3T, contrast amplification compared to TIs equal to 15 times). The gray-scale shows T_1 values over a range from 780 ms (i.e., 540/ln 2 ms) to 924 ms (i.e., 640/ln 2 ms) with the dark low signal representing shorter normal T_1 values of about 780 ms and higher signal representing abnormal T_1 values up to a maximum of about 924 ms. Lesions with T_1 values greater than the maximum in the mD "overshoot" (i.e., greater than about 924 ms) and appear mid-gray in their centers (where their T_1 values are unreliable). The T_1 maps of lesions that overshoot are surrounded by high signal boundaries. The T_1 maps are only valid in the mD and are obtained using long TR IR images, as in this case. If TR is short, the T_1 values may be too low and need to be corrected. dSIR, divided subtracted inversion recovery.

https://dx.doi.org/10.21037/qims-22-394